# Calibrating some Rock Physics Relations to Brazilian Rocks in the Lab

*Guilherme Vasquez, Lúcia Dillon, PETROBRAS/CENPES, Raquel Velloso, FADESP, Brazil.*

**Abstract**

Over the last 60 years or so, many rock physics theoretical and empirical relations had been proposed and applied as a guide to seismic and log interpretation. With the recent advances in AVO processing and interpretation and elastic inversion, these rock physics transforms had proven to be powerful tools to the explorationists.

Among these transforms there are some theoretical models that establishes physically based relations between petrophysical rock properties to its seismic behavior, but usually it depends on many parameters related to rock and pore structure and composition. On the other hand, there are numerous empirical or semi-empirical relations that require easily obtained parameters, but generally are strictly valid only on particular rock types similar to those used for the transform deduction.

On this paper we discuss some popular rock physics relations and propose modifications to typical and important Brazilian rocks based on laboratory measurements.

**Introduction**

As geophysicists we get only few information about reservoirs. We know something about its geometry from seismic transit time and we try to obtain every information we can from seismic amplitude and velocities. But our colleagues geologists and reservoir engineers don't care about transit time and velocity, and they are right.

Nowadays there's a lot of techniques, much of them combining seismic and log data or even a priori models, trying to extract useful information from seismic data. Geostatistical methods, volumetric AVO interpretation and inversion, and elastic inversion are some tools that had been used to get litologic and fluid information.

Although these are powerful tools, we must have in mind that we start with nothing better than a seismic and well log data set. So, it's very important to calibrate first our rock and well data, ensure that we are confident about our logs, before we can calibrate seismic and well data. Even if we deal with techniques that doesn't involve well data, it's better to know first the relations between the desired petrophysical properties and the observed seismic behavior.

In this scenario, a lot of rock physics relations have emerged. Generally the most famous includes velocity-porosity relations, velocity-density and velocity-clay content relations and also compressional to shear velocities relations. Among the recent contributors on literature we can point out Batzle, Castagna, Han, Mavko, Nur, Tosaya, Yin and their associates. Although a general formula is very useful, it's important to refine the rock physics relations to our particular case as much as we can. It's common to find out that some bias on porosity, diagenesis, fracturing or mineralogy leads to one peculiarity in the rock physics transform.

On PETROBRAS activities in AVO, acoustic, elastic and geostatistical inversion, we have found out that usually we can do a much better job not discarding, but adapting some literature relations to the target field, specially if we have one amount of information that is too expressive to throw out, but too small to construct more elaborated models.

On this paper we present some cross checking examples from PETROBRAS Rock Physics Laboratory data and the literature regressions, pointing out some discrepancies, maintaining our confidential rights.

**Shear to Compressional Velocities Relations**

In our day-to-day work we deal with seismic volumes that register the P wave arrivals, but it's well known that non-zero offset data carries shear wave velocity information. Also, if we try to calibrate these data with well logs, we will notice that there are a lot of wells that doesn't contain shear wave sonic log, or it is restricted to a small depth range.

In spite of some neural network and multivariate panaceas, the Greenberg-Castagna method has proven to be a very useful and reasonable approach to obtain shear wave velocity. Obviously, sometimes it fails on particular cases, especially if we have some mineralogical peculiarity. There are a lot of examples where just one laboratory based adjustment of the original equations gave very good results.

Figure 1 presents the crossplot between Vp and Vs for some water-saturated Brazilian sandstones, along with the Greenberg-Castagna line for pure-quartz sands. Each symbol represents a different reservoir. We would like to point out that the red points corresponds to Terciary sands, while every other data refers to Cretaceous sandstones. It's curious that one particular Cretaceous sand (the blue

points) behaves just like the Terciary one. The crossplot in figure 2 was obtained after calibrating the Greenberg-Castagna coefficients for one particular reservoir. There the measured and predicted shear wave velocities over all the geologic column are presented. Note that one interval, which contains igneous rocks, falls a little bit far from the perfect prediction line.

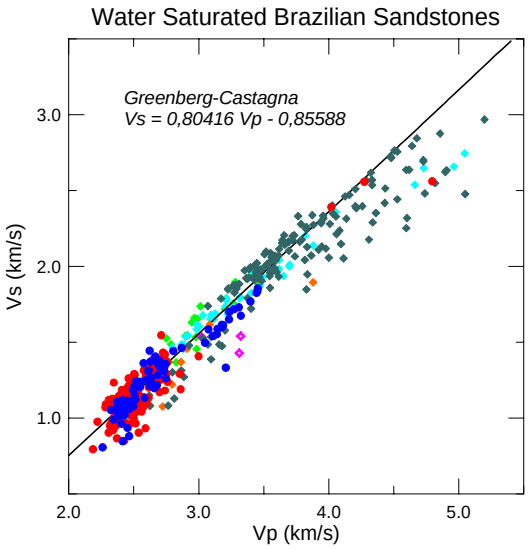


Figure 1 - Vs-Vp cross plot for some water saturated Brazilian sandstones. The line represents the Greenberg-Castagna equation for sandstones.

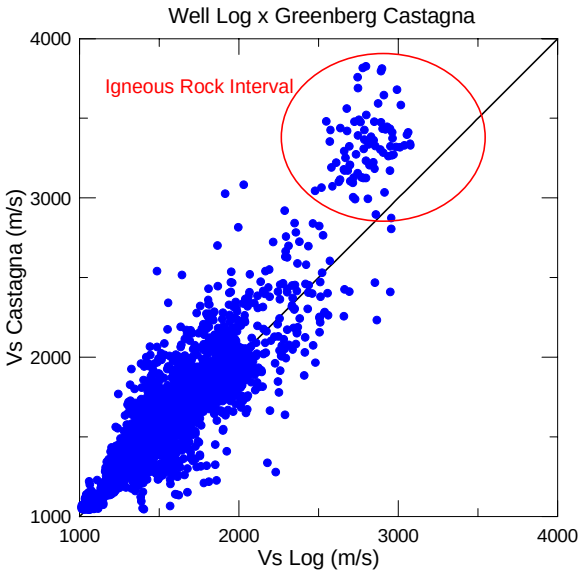


Figure 2 - Shear velocity from sonic log and obtained by Greenberg-Castagna calibrated. The line represents perfect prediction.

Figure 3 presents the comparison for the Krieff's prediction and the measured shear wave velocities for 174 Brazilian limestone samples. Note that Krieff's method does a fairly good job, although it tends to give systematic lower shear wave velocities.

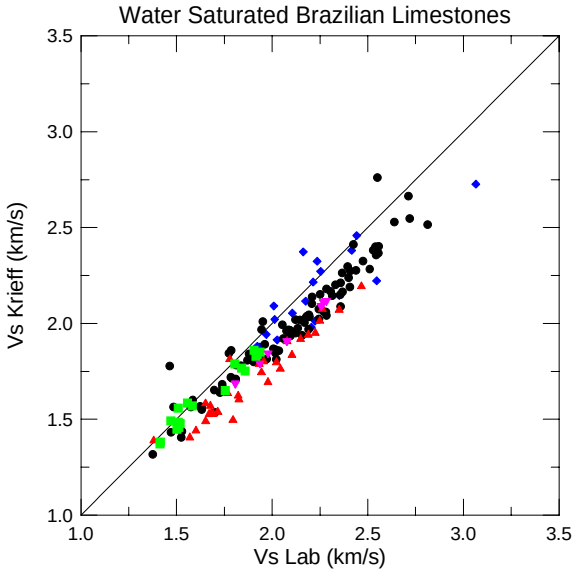


Figure 3 - Shear wave velocities of water saturated Brazilian limestones measured and predicted by Krieff's method. The line represents perfect fit.

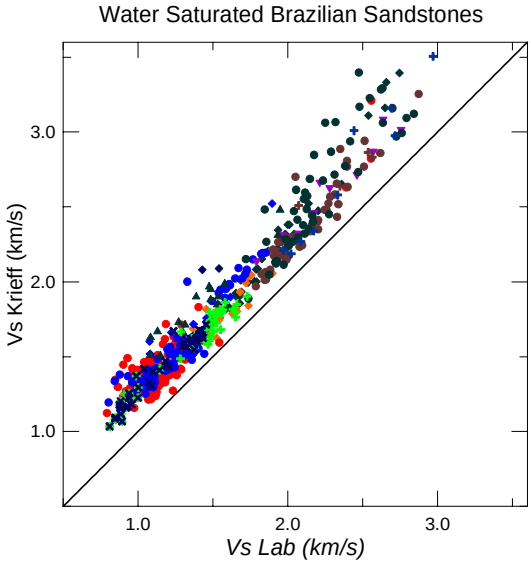


Figure 4 - Measured and Krieff's prediction for Vs on water saturated Brazilian sandstones.

Observing figure 4 we may notice that the Krieff's method doesn't work so well for sandstones, and tends always to give a higher shear wave velocity than the real value.

### Velocity-Porosity Relations

Since the fifties people try to deduce or infer useful velocity-porosity relations. Wyllie's time-average equation was conceived to obtain porosity from sonic log, and is still used, although not always recommended, to obtain porosity form seismic data in deterministic or even sthocastic inversions. In fact, many other authors, like Raymer *et al.* (1980), Han *et al.* (1986), had proposed other equations to predict velocity from porosity or vice-versa. Particularly the Nur's critical porosity concept are quite attractive because of its inherent physical coherence. Also, we cannot forget models like those from Dvorkin and Nur (1996). It is recommended to draw specific velocity-porosity laws for the case under study, instead of applying general laws, if we have a representative data set. Figure 5 presents one example for Brazilian limestones.

It is curious to note the similar acoustic impedance to porosity correlation observed on two different Brazilian sands, one Cretaceous and other Terciary age, as illustrated in figure 6.

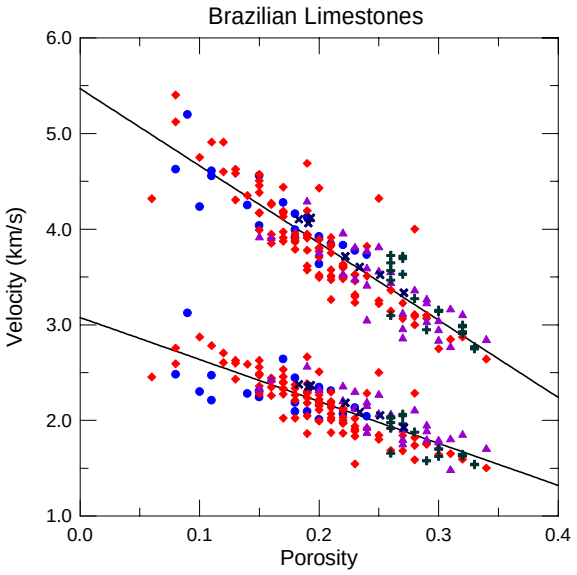


Figure 5 - Velocity-porosity relation for dry Brazilian limestones.

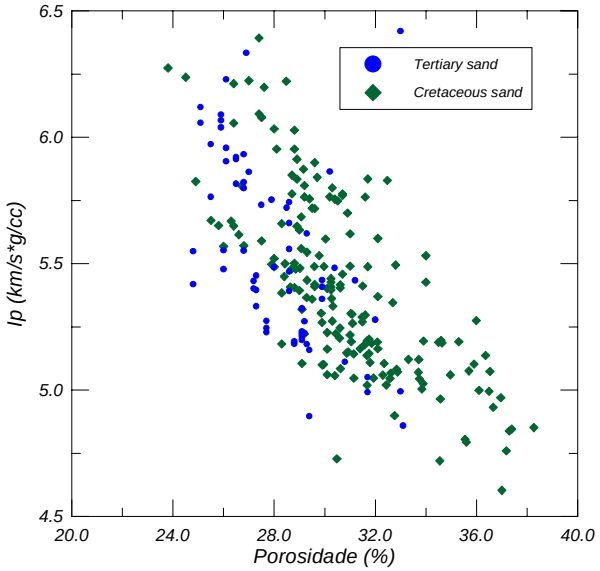


Figure 6 - Comparison of acoustic impedance of two particular Brazilian sands.

### Velocity-Density Relations

We are always handicapped when dealing with seismic data. In spite of it's large, continuous coverage, and although amplitudes are related to impedance, we cannot obtain a real impedance measurement. The best we can do is to infer contrasts. So, it's good to know some velocity to density relations to refine our interpretation and inversion projects. The famous and effective Gardner equation can be used, or the new proposals from Castagna, but, again, if we know something about our rocks, we have to use it.

Figure 7 shows a cross plots between compressional wave velocity and density for water saturated Brazilian sandstones in which each different symbol represents one case. It can be notice that the Castagna's proposed equations could give a good estimation for densities but, again, we can make it better by calibrating the equation to our target reservoir.

### Velocity Permeability

Although it's not physically justified, sometimes we are quite lucky to have a good velocity-permeability relation. The plot on figure 8 shows a blind test where we had put the permeability log obtained form velocity and porosity logs with absolute permeability data obtained from core samples. This particular well was not used on the construction of our velocity-porosity-permeability function. In this case we know that the particular diagenetic history of the reservoir is responsible for this good correlation:

the decrease in reservoir permeability are due to calcite cementation, that leads also to higher velocities.

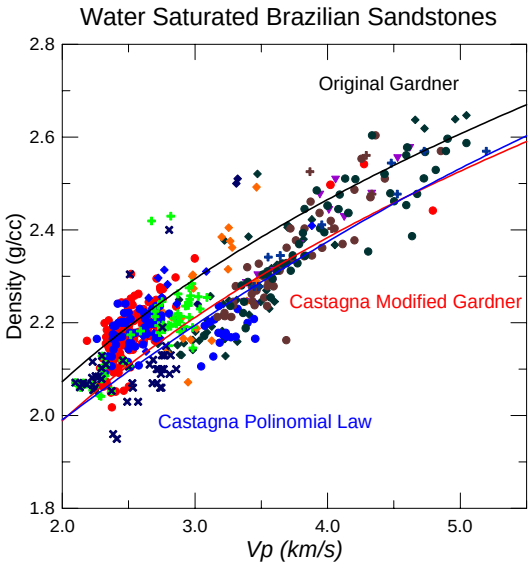


Figure 7 – Velocity-density cross plots for Brazilian sandstones.

## Conclusions

As shown here with some examples, although some general rock physics transforms can predict some petrophysical to seismic properties correlations in Brazilian rocks, a more detailed analysis can be done by calibrating these relations to particular fields.

## References

Castagna, Batzle and Kan, T. K., 1993. Rock physics – The link between rock properties and AVO response, *in Offset-Dependent Reflectivity – Theory and Pactice of AVO Analysis*, J. P. Castagna and M. Backus eds., Investigations in Geophysics No8, Society of Exploration Geophysicists, Tulsa, Oklahoma, 135-171.

Dvorkin, J. and Nur, A., 1996. Elasticity of high-porosity sandstones: theory for two North Sea data sets, *Geophysics*, 61, 1363-1370.

Gardner, G.H.F., Gardner, L.W., and Gregory, A.R., 1974. Formation velocity and density – The diagnostic basis for stratigraphic traps. *Geophysics*, **39**, 770-780.

Han, D., Nur, A., Morgan, D.,1986. Effects of porosity and clay content on wave velocities in sandstones, *Geophysics*, **51**, p.2093-2107.

Nur, A.; Marion, D. And Yin, H, 1991. Wave velocities in sediments, In*: Shear Waves in Marine Sediments, p. 131-140,* J. M. Hovem et al. (eds.), Kluwer Academic Publishers.

Raymer, L. L.; Hunt, E. R., Gardner, J. S., 1980. An improved sonic transit time-to-porosity transform. SPWLA 21ST ANNUAL LOGGING SYMPOSIUM, July 8-11.

Wyllie, M. R. J, Gregory, A. R., Gardner, G. H. F., 1958. An experimental investigation of factors affecting elastic wave velocities in porous media. *Geophysics*, **23**, p.459-493.

## Acknowledgments

Thanks to Petrobras for supporting and permission to publish this work. The authors would like to thanks also Guenther Schwedersky and Theogenes Oliveira for revision and suggestions.

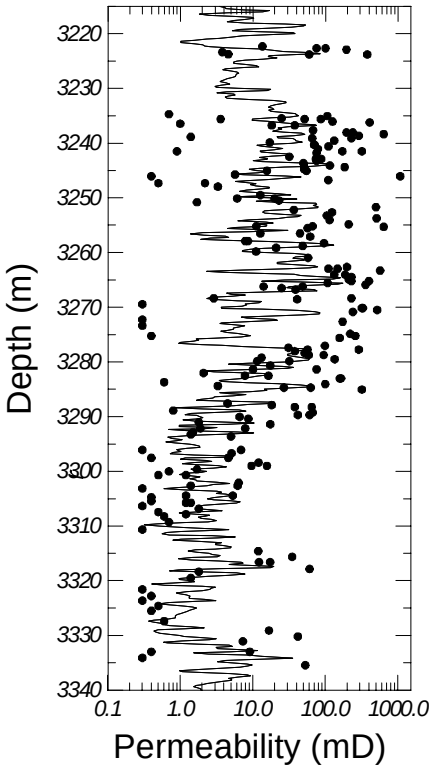


Figure 8 – Permeability log obtained from porosity and sonic logs.

# Identifying rock failure mechanisms through shear wave velocity measurements

*José Agnelo Soares, Federal University of Rio de Janeiro,* agnelo@igeo.ufrj.br
*Antônio Cláudio Soares, PETROBRAS Research Center,* aclaudio@cenpes.petrobras.com.br

**Abstract**
Shear wave velocities are used here as an indicator for failure mechanism contributions in rock compressive tests. Eleven high porosity carbonate samples are tested with shear wave velocity monitoring. Eight of them follow forced linear confining-deviatoric stress paths while the remaining three are uniaxial strain tests. Using the shear velocity profile acquired on each test and a pre-defined model for shear failure, it was possible to analyze the contribution of failure mechanisms: shear failure and pore collapse.

## Introduction

High porosity reservoirs offer ideal conditions for development of pore collapse, as showed by Soares (2000). Such rock failure mechanism may be the cause of some known production field subsidence and abrupt decreasing on production rates.

As described by Scott Jr et al. (1998), among main rock strain mechanisms are elastic deformation, dilatance, pore collapse and normal consolidation. Elastic deformation occurs at low stress levels and does not cause reservoir damage. Dilatance occurs mainly at low confining pressure and high deviatoric stress and it is accompanied of intense rock micro fissuring and increase of rock volume. In compression triaxial tests, dilatance occurs after elastic deformation and immediately before shear failure. Pore collapse occurs mainly on highly porous sandstone or limestone, under high stress levels, but insufficient to reach the shear failure envelope. This failure mechanism involves rupture of grain-grain contacts, which results in collapse of the whole porous framework. Normal consolidation occurs after the collapse of pores, with grain rearrangement, constant decrease of porous volume and, as a consequence, rock compaction.

All these reservoir deformation phases may be monitored through measurements of wave velocities. Scott Jr et al (1998) show how these phases may be recognized in a wave velocity profile. During elastic deformation there are closing of microfissures and all possible grain-grain contacts are done. This results in an approximately linear increase of wave velocities. Dilatance, which immediately precedes shear failure, strongly diminishes the shear velocity gradient. On the other hand, pore collapse mechanism includes loss of rock cohesion due to cement rupture. This damages grain-grain contacts and, as a consequence, wave velocities decrease. This pore collapse effect is especially observed for shear wave velocity.

The mechanism which dominates rock failure, shear or pore collapse, depends on the relationship between the effective confining pressure (hydrostatic) and the tectonic stresses (deviatoric). Paths of stresses with low confining to deviatoric stress ratio, preferably induces rock shear failure, while high confining to deviatoric stress ratio tends to induce rock pore collapse. Triaxial tests, with constant confining pressure, can lead to shear failure or pore collapse, depending on the confining pressure level. Low confining pressure leads to shear failure while high pressures induce pore collapse. Uniaxial deformation tests, where confining pressure is increased according the rate need to avoid lateral sample expansion, have a non-linear stress path. This is an intermediate path between those of hydrostatic and triaxial tests, and as a consequence, can lead to shear failure, pore collapse, or a sum of contributions of both failure mechanisms.

Simply analyzing how shear velocity varies along rock mechanics tests, it is possible to identify the point of rock failure. To clearly identify the dominant mechanism of rock failure, however, it is necessary an additional information. Here it was used a function which defines the shear failure envelope, according the non-linear Mohr-Coulomb criterion (Soares & Dillon, 2000). This function defines the shear failure envelope in terms of rock dynamic shear modulus and confining pressure. Comparison between the stress path and the shear failure envelope, for each test, identified whether the failure was primarily due to the shear failure or pore collapse contribution.

## Laboratory tests

Eleven core samples, extracted from a 70m thick carbonate interval, were tested. Rock samples were cylinders around 2in long and 1.5in of diameter. Before tests, they were cleaned, dry and saturated with mineral oil. Relative depths to the shallowest sample (9102) and lab-measured porosities are presented in Table 1.

To analyze the influence of stress paths on occurrence of pore collapse, pre-defined linear paths of stress were adopted for eight tests, while the three others were uniaxial deformation tests, what means non linear stress paths. Figure 1 presents the stress path for each sample/test.

# Identifying rock failure mechanisms through shear velocity

## Results

To identify the predominant failure mechanism of a given test, it was plotted, in the same frame, the stress path, the shear velocity profile and the shear failure envelope. After Soares & Dillon (2000), the ultimate rock strength $\sigma_1^{ef}$ may be expressed as a function of the effective confining pressure $\sigma_3^{ef}$ and the dynamic rock shear modulus $G_d$ as

$$\sigma_1^{ef} = \frac{-b + \sqrt{b^2 + 4a\sigma_3^{ef}}}{2a} + dG_d + e(G_d)^2$$

where **a**, **b**, **d** and **e** are regression coefficients. For carbonates **a** = 0.000892, **b** = 0.588805, **d** = 0.855462 and **e** = 0.309565. Stresses are given in MPa and $G_d$ is in GPa. Deviatoric stress is the difference $\sigma_1^{ef}$ - $\sigma_3^{ef}$, and so, the shear failure envelope may be computed for the confining / deviatoric stress plane.

Figure 2 and Figure 3 show, for each tested sample, the stress path (red), the shear failure envelope (black) and the shear wave velocity profile (blue). In these figures, stress paths and shear envelopes have coordinate values on the left axis while shear velocity profiles have coordinate values on the right axis. Vertical segmented lines indicate the point of rock failure, as suggested by shear velocity profiles.

In Figure 2, tests of rock samples 9102, 9162, 9120, 9144, 9177 and 9147 show initial decrease on shear velocity over the confining pressure indicated by segmented lines, indicating failures. In these tests, stress paths do not yet achieved the shear failure envelope at failure. Therefore, for tests on Figure 2, failure occur primarily due to pore collapse.

Tests of samples 9138, 9129, 9020, 9135 and 9159, showed in Figure 3, do not show decreasing of shear velocities, instead, sometimes show a shear velocity threshold when the stress path crosses the shear failure envelope. This is an indication that in these tests the dominant mechanism was shear failure.

Should be noted that stress paths of Figure 3 have higher inclination than those of Figure 2, and shear velocity profiles in Figure 3 do not show decreasing at the point of failure, as those of Figure 2. Therefore, pore collapse would be the dominant failure mechanism only for low inclination stress paths.

## Conclusions

Based on these results we conclude that the dominant failure mechanism is mainly defined by the stress path. High confining pressures with low deviatoric stresses lead to pore collapse, while low confining pressures with high deviatoric stresses lead to shear failure. Shear wave velocity monitoring permits the identification of both failure mechanisms.


## Acknowledgements

Authors are grateful to PETROBRAS for the opportunity of this research and publication. Thanks to Júlio César Beltrami for sample preparation, Sérgio Murilo and Marcos Dantas for test conduction, and Lincoln Homero for velocity measurement assistance.


## References


Scott Jr., T.E., Zaman, M.M., Roegiers, J.C. (1998) Acoustic-velocity signatures associated with rock-deformation processes. Journal of Petroleum Technology, June 1998, 70.

Soares, A.C. (2000) Um estudo experimental para definição de colapso de poros em rochas carbonáticas. Tese de mestrado. COPPE/UFRJ.

Soares, J.A., Dillon, L.D. (2000) Deriving cohesion and angle of friction from well logs. 31st International Geological Congress. Rio de Janeiro.


**Table 1** – Samples relative depth and porosity.

| Sample Reference | Relative Depth (m) | Porosity (%) |
|---|---|---|
| 9102 | 0.00 | 30.2 |
| 9020 | 0.30 | 31.4 |
| 9120 | 33.05 | 31.4 |
| 9129 | 35.90 | 31.9 |
| 9135 | 37.75 | 23.7 |
| 9138 | 38.65 | 24.0 |
| 9144 | 40.80 | 28.9 |
| 9147 | 41.80 | 27.6 |
| 9159 | 46.10 | 25.1 |
| 9162 | 47.20 | 30.2 |
| 9177 | 52.75 | 31.1 |

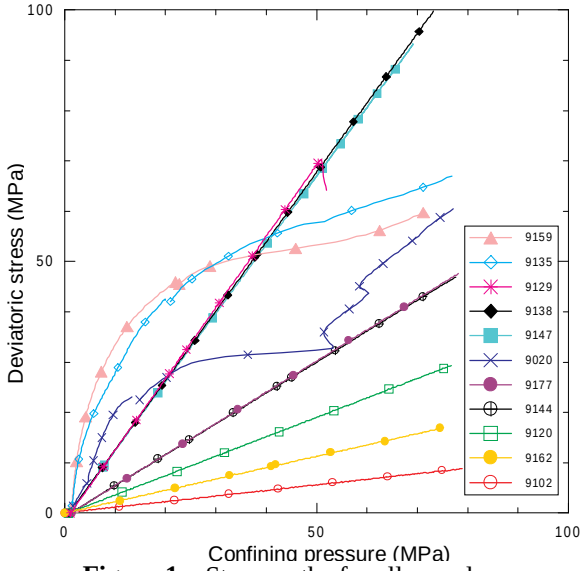


**Figure 1** – Stress paths for all samples.

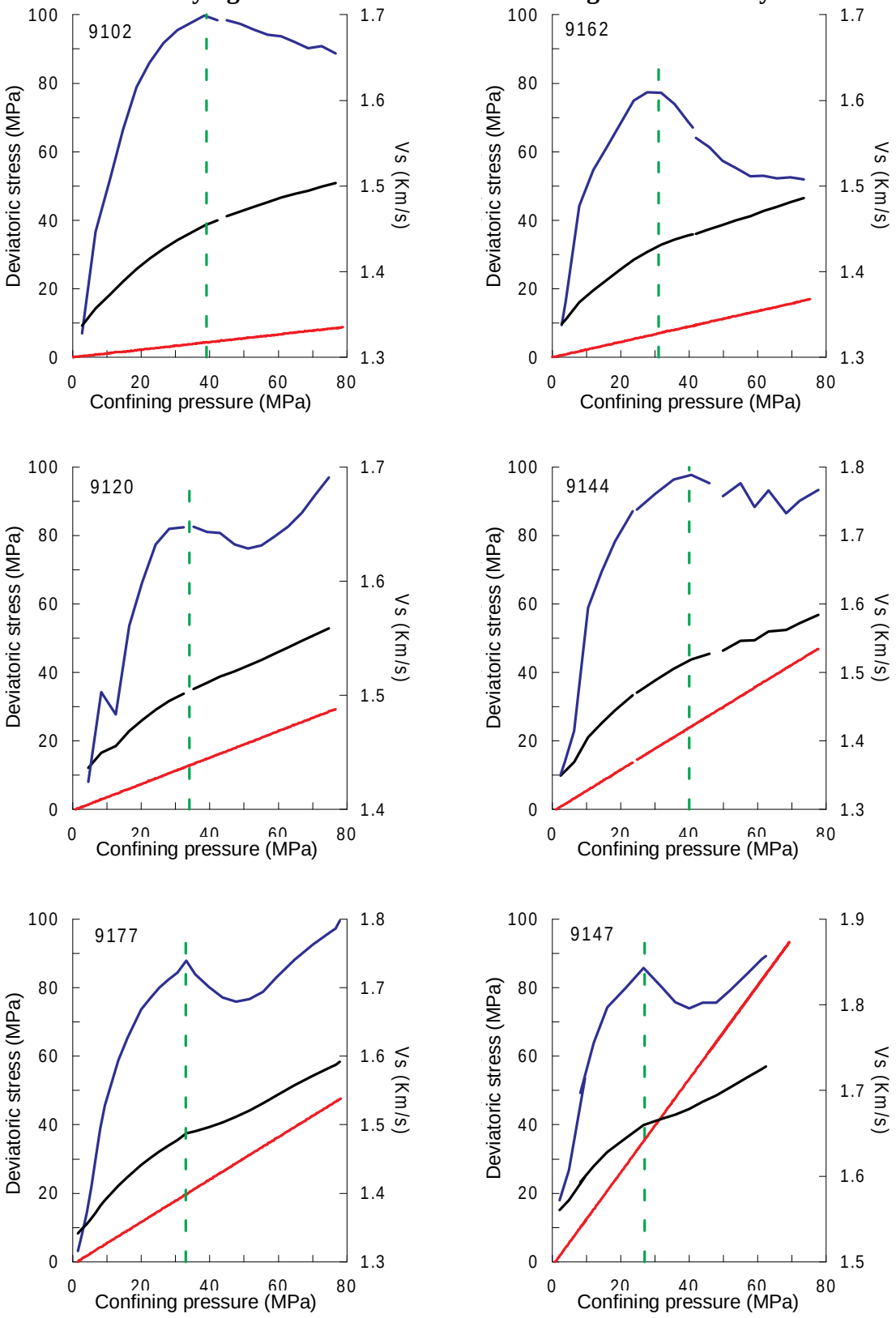


**Figure 2** – Failure indication by Vs variation (segmented), stress path (red), Vs profile (blue) and shear failure envelope (black) with increasing confining pressure and inclination of stress path.

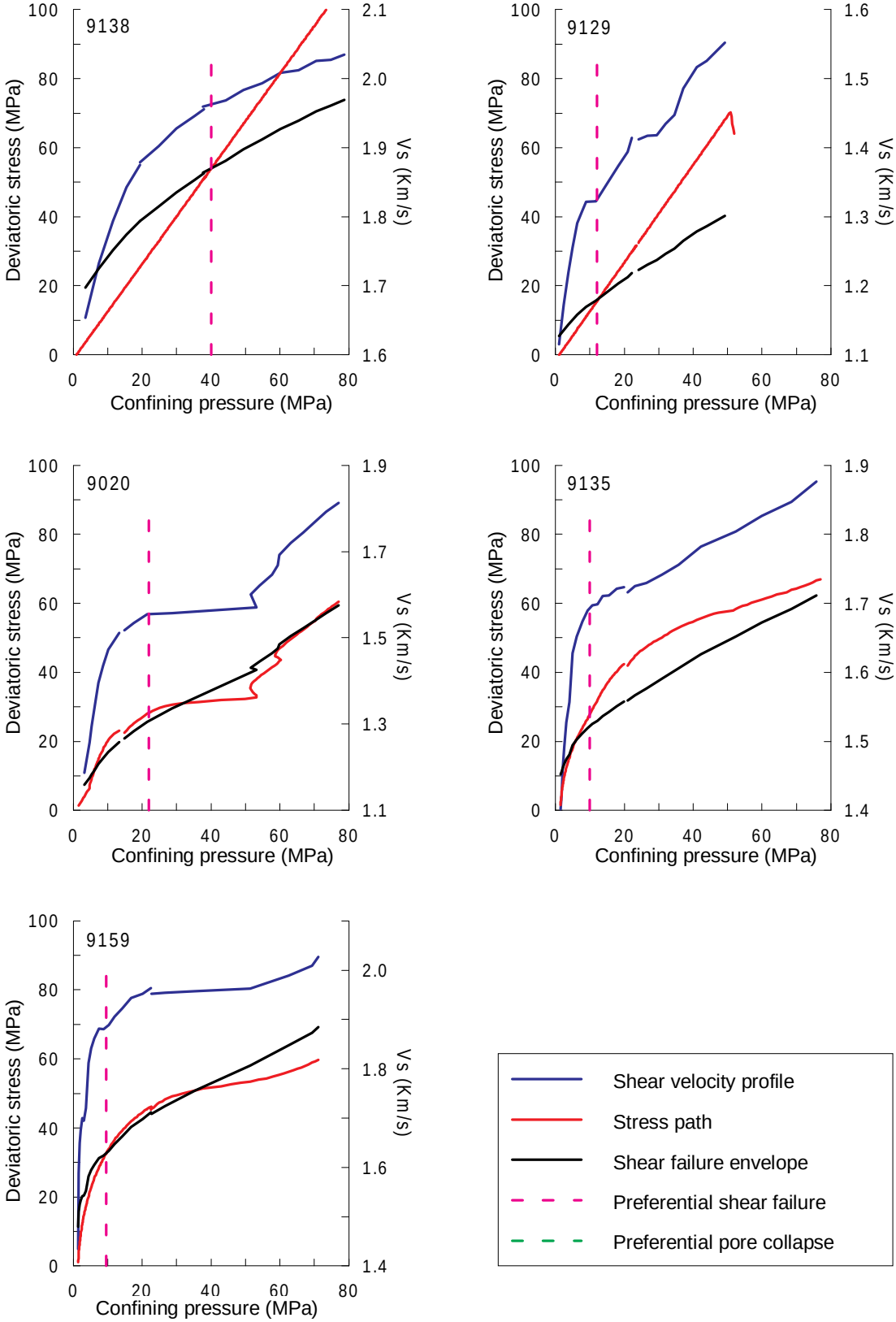


**Figure 3** – Failure indication by Vs variation (segmented), stress path (red), Vs profile (blue) and shear failure envelope (black) with increasing confining pressure and inclination of stress path.

# Perfis sintéticos de Vs: Greenberg Castagna x Redes Neurais

*José E.Ferrer Pinheiro e Guilherme F. Vasquez PETROBRAS S/A, Brasil*

ABSTRACT

Advantages of using shear waves have already been known for a long time, specially when used together with compressinal waves. Applications include wellbore stability analysis, gas detection, evaluation of formation anisotropy, interpretation and calibration of AVO analysis. Specifically with AVO modelling, when shear-wave logs are not available or when doubts about log accuracy arise, it is possible to predict the Vs logs using some of the models published in literature. In this paper, using data from two offshore wells, we compare the performance of two models for predicting Vs: the well-known Greenberg-Castagna and an artificial neural networks method named backpropagation. Each method showed advantages and limitations and depending on the quality of preliminary information available one of the methods can prevail over the other.

## INTRODUÇÃO

A informação da onda S tem um papel fundamental numa série de aplicações, possibilitando entre muitos benefícios a identificação de fluidos e de litologias e a interpretação e calibração das respostas de AVO (*Amplitude versus Offset*). Por uma miríade de motivos o perfil de onda S pode não estar disponível ou então pode ter a sua qualidade comprometida, seja pelas limitações das ferramentas ou por problemas relacionados ao próprio poço. Devido a esses problemas e também pela crescente demanda por calibrações de análise de AVO surgiram vários métodos de geração perfis sintéticos de onda S. Em 1997, Lira et al. realizaram um estudo comparativo entre a técnica de Greengberg-Castagna (GC), Krief e as relações Vp x Vs obtidas de medições laboratoriais de amostras de rocha para quatro poços *offshore* brasileiros. Observaram que GC obteve resultados superiores ao método de Krief nesta área, sendo, no entanto, inferiores aos resultados obtidos com as relações geradas a partir de dados de laboratório. Todavia, devido ao alto custo envolvido na testemunhagem, as amostras de rocha estão disponíveis apenas em alguns poços, e mesmo nesses poços a amostragem é restrita a pequenos intervalos, e conseqüentemente limitando as relações VpxVs a esses intervalos. Por isso, e também com o objetivo de buscar sempre soluções cada vez mais precisas, novos métodos têm sido testados e suas performances constantemente comparadas com os modelos já estabelecidos. Neste sentido o método de Greenberg-Castagna é comparado com uma ferramenta que tem tido uma grande aplicação nos mais diversos campos do conhecimento e destacando-se por sua capacidade de solucionar problemas não lineares: as redes neurais.

## GREENBERG-CASTAGNA

Greenberg e Castagna (1992) desenvolveram um método de geração de perfis de Vs a partir de relações empíricas estabelecidas com base em perfis e em dados de laboratório entre Vp e Vs para rochas mononinerálicas (arenito, dolomita, calcita e argila) saturadas com salmoura. O método consiste basicamente em se determinar de forma iterativa valores de Vp e Vs para rochas saturadas com salmoura que são então levados à condição de saturação da rocha *in situ* através da técnica de substituição de fluidos (Equações de Gassmann, 1951) gerando dessa forma um perfil calculado de Vp e de Vs. Esse processo se repete até que até que as velocidades compressivas calculadas gerem valores de Vp similares aos do perfil segundo algum critério de convergência. Atingido o critério, considera-se determinado o perfil de Vs para a saturação *in situ*. Este método requer o conhecimento da litologia, saturação e dos módulos elásticos e densidade dos constituintes minerais e dos fluidos saturantes

## REDES NEURAIS

Redes neurais são métodos computacionais não lineares que não requerem um modelo matemático inicial para obter a solução de um problema. É recomendado na solução de problemas complexos, onde a incógnita que se quer determinar é função de uma série de fatores inter-relacionados. A idéia básica é que a rede é capaz de aprender a solução após ser apresentada a um conjunto previamente selecionado de dados de entrada e saída. Durante o processo de aprendizado é importante o acompanhamento da performance da rede utilizando para tal critérios de convergência bem definidos, pois a partir de um certo ponto ela começa a memorizar a resposta e, dessa forma, a perder sua capacidade de generalizar, ou seja, sua habilidade de produzir resultados precisos quando apresentada a um conjunto diferente de dados. Para confirmar a aplicabilidade da rede gerada, após o treinamento a rede é testada com um novo conjunto de dados e só então,

ao obter resultados satisfatórios, a rede é realmente aprovada. A arquitetura de rede empregada neste trabalho é a Backpropagation (BP), que por ser a mais bem compreendida do ponto de vista matemático e operacional, é a mais utilizada no mundo. Detalhes sobre o funcionamento deste tipo de rede pode ser encontrado em Wassermann (1989).

## RESULTADOS

### POÇO A

#### Greenberg-Castagna

A partir dos dados de litologia, saturação e do perfil de Vp calculamos o perfil sintético de Vs para dois poços da área utilizando a técnica de GC. O resultado para o poço A, onde foi corrida a ferramenta DSI, pode ser visto na figura 1. Observa-se que o perfil calculado apresenta uma boa concordância com o perfil original, exceto no reservatório. A razão para esta discrepância pode ser devido a ocorrência de invasão por filtrado de lama ou por uma imprecisão na quantificação da saturação. Uma indicação da invasão da formação pelo filtrado de lama é a diminuição do diâmetro do poço observado no perfil de Caliper, causada pela formação do reboco na parede deste. Outra é a comparação dos perfis de resistividade LLD e LLS.

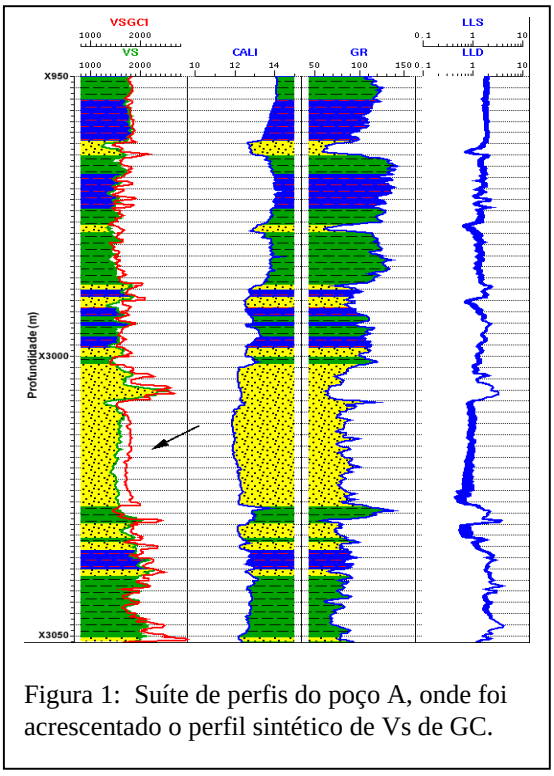


Figura 1: Suíte de perfis do poço A, onde foi acrescentado o perfil sintético de Vs de GC.

Como a ferramenta de Vp tem pouca profundidade de investigação, é comum que ela meça porções da rocha que estão pelo menos parcialmente invadidas pelo filtrado. Baseado nestas considerações e no fato de que o perfil de Vs é estimado a partir de VP, calculou-se um novo perfil de Vs, sendo que a condição de saturação informada foi de uma formação totalmente invadida. O resultado pode ser visto na Figura 2. Aqui temos o perfil original e o novo perfil de G.C, com a condição de invasão informada. Observa-se que agora há uma boa amarração entre os dois perfis. A correlação entre eles é de 87 % neste intervalo. Este resultado é uma indicação de que o método de GC pode ser uma ferramenta de controle de qualidade dos perfis obtidos por ferramentas dipolares quando o volume dos constituintes litológicos e a saturação são informados corretamente.

#### Back Propagation

A BP que empregamos para obter o perfil de onda S é constituída por duas camadas internas e tem como dado de entrada o perfil de onda P e o perfil de raios gama. O perfil de onda P é um parâmetro "natural", uma vez que tanto Vp quanto Vs são afetados de

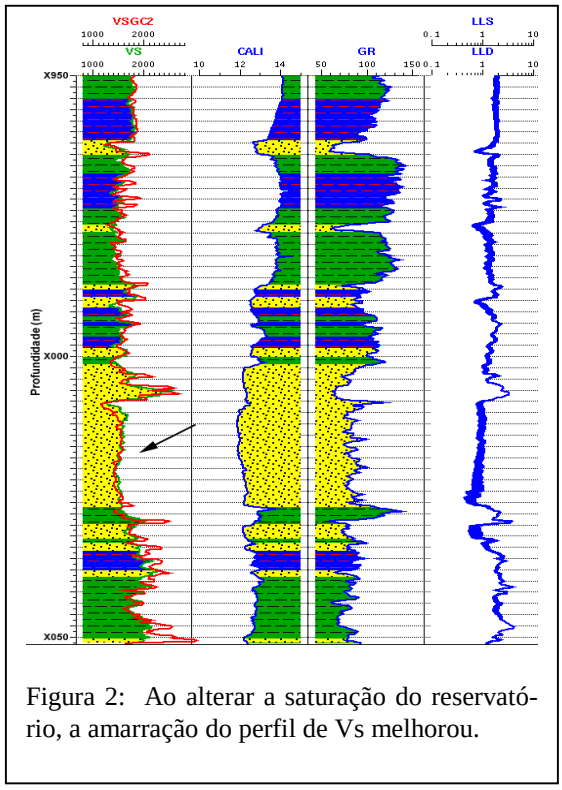


Figura 2: Ao alterar a saturação do reservatório, a amarração do perfil de Vs melhorou.

forma similar pela litologia e pela porosidade. Somese a isso o fato do perfil de Vp estar disponível em praticamente todos os poços dessa área. Quanto ao perfil de raios gama, é de conhecimento geral que a quantidade de argila é um fator que também influencia bastante a velocidade da onda cisalhante. (Han et al.,1986). No processo de treinamento da rede foram tomados cuidados na seleção de dados que fossem representativos das litologias encontradas e sem problemas ambientais. Foram utilizados dois poços no treinamento, sendo que em um deles a ferramenta de sônico utilizada foi o DSI enquanto que para o outro poço foram corridas as ferramentas X-MAC e DSI, sendo porém em intervalos distintos. Na etapa seguinte quando se avaliou a aplicabilidade da rede foram empregados mais dois poços, onde em cada um deles foi corrida uma ferramenta diferente.

Para o poço A obteve-se um resultado ligeiramente inferior ao do método de GC. Como pode ser visto na Figura 3 o método de BP no trecho do reservatório onde há o problema da invasão da formação amarrou bem com o trecho do perfil contaminado. Isto ocorreu mesmo treinando somente com porções do poço sem problemas ambientais, pois no momento de se gerar a solução esta é dada a partir de um perfil de Vp que tem trechos registrados dentro da zona invadida.

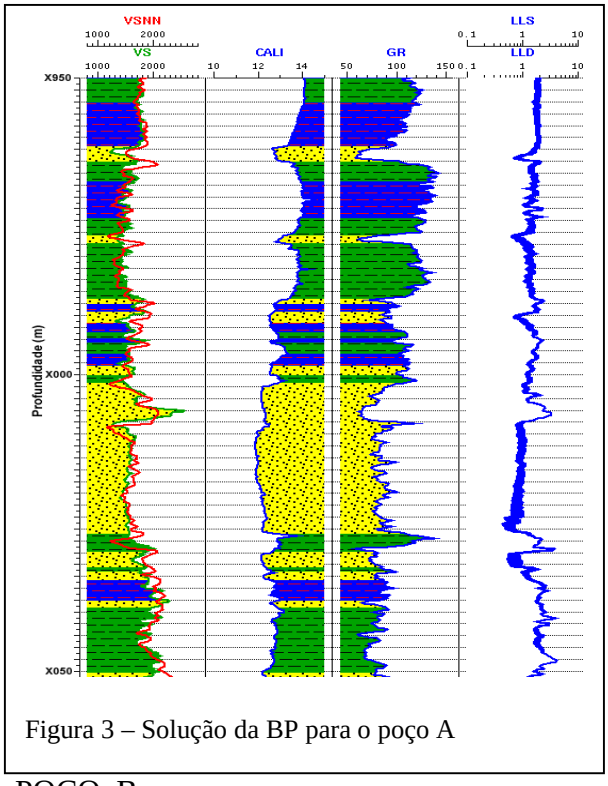


Figura 3 – Solução da BP para o poço A

POÇO B

Greenberg-Castagna

Na Figura 4 temos os dois perfis de VS do poço B para comparação: o obtido pela ferramenta X-MAC e o calculado pela técnica de GC. Valores mais altos de Vs correspondem a ocorrência de diabásio, que ficou bem marcado no perfil de GC. No perfil calculado o contraste de velocidade entre o arenito e a rocha sobreposta a esta é menor que o que se observa no perfil de campo. Para o arenito os valores calculados foram superiores ao do perfil, ocorrendo o comportamento inverso para as argilas. Porém é importante observar que o perfil sintético conseguiu prever a quebra na velocidade. Quanto à causa da discrepância entre os perfis, esta pode estar relacionada a uma descrição litológica simplificada, o que levaria a imprecisões no calculo da Vs pelo método de GC.

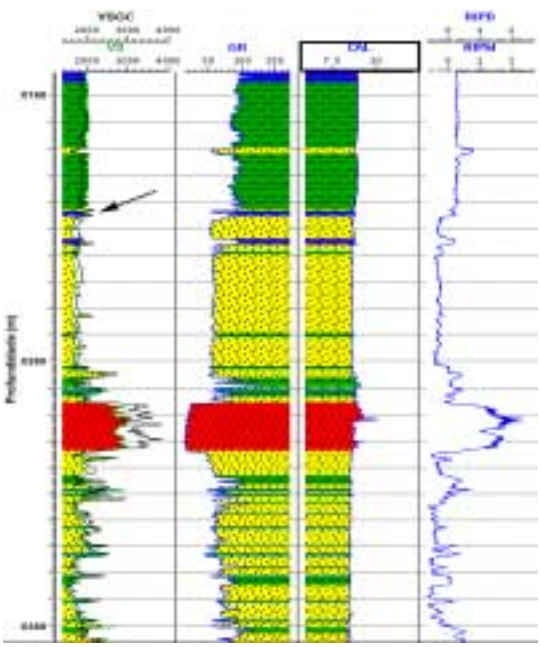

Figura 4: Perfis do Poço B onde se compara o perfil sintético de Vs de GC com o original.

Back Propagation

Na geração do perfil sintético via Back Propagation foi aplicada a rede obtida anteriormente. Para o poço B a resposta gerada foi um pouco melhor que a obtida pelo método de GC, exceto no nível do

diabásio. Observando-se a Figura 5, nota-se que o método de BP não conseguiu identificar o diabásio. Esse resultado é função da informação disponibilizada durante o treinamento, quando nenhum dado deste litologia foi apresentado à rede. No restante do perfil estudado a amarração do perfil gerado foi muito boa, mesmo no intervalo acima do diabásio onde o método de GC não funcionou bem.

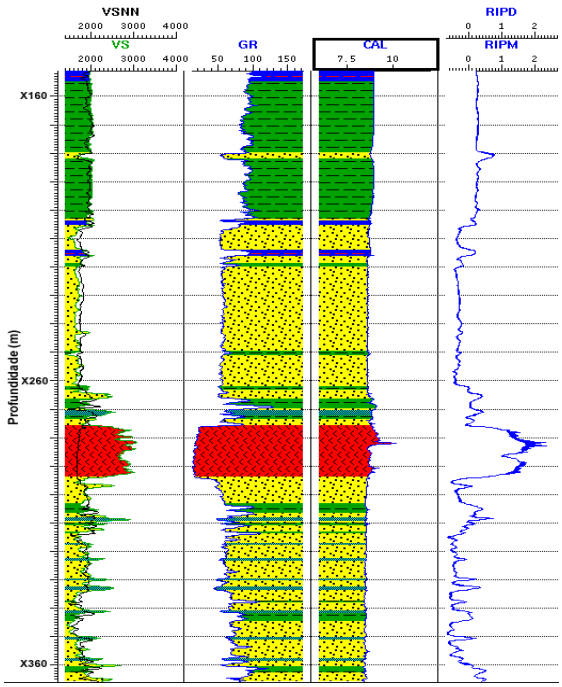


Figura 5: Suíte de perfis do poço B junto com a solução da BP para Vs.

## COMENTÁRIOS

Observou-se que o método de Greenberg-Castagna pode ser muito útil mesmo quando o perfil de Vs existe, pois pode servir como uma ferramenta de controle de qualidade deste. No caso do poço A o perfil sintético indicou problemas que poderiam estar ligados à invasão de filtrado ou na informação da saturação do perfil. A análise de outros perfis disponíveis permitiu esclarecer a situação. Ainda sobre este método, a solução gerada vai depender sempre da aplicabilidade da teoria de *Biot-Gassman* e da qualidade da informação necessária *a priori*, como a litologia e a saturação.

O método de redes neurais também apresentou resultados satisfatórios, porém a sua aplicabilidade depende da disponibilidade de poços com perfis de Vs de boa qualidade para as fases de treinamento e teste e também da representatividade dos dados apresentados à rede. A presença de perfis de diferentes companhias de serviço não foi um problema uma vez que havia dados suficientes para caracterizar as duas ferramentas. Uma possível vantagem deste método é que uma rede treinada apenas com perfis que por suas características técnicas lêem além da zona invadida poderia gerar perfis não contaminados.

Por outro lado, por tratar-se de um método determinístico, no modelo de Greenberg-Castagna tem-se um maior controle das incertezas do resultado. Inclusive, segundo Wasserman (1989), toda rede possui um certo grau de imprevisibilidade.

## REFERÊNCIAS

Gassmann, F., 1951, Elastic waves through a packing of spheres: Geophysics, 16, 673-685.

Greenberg, M. L., and Castagna, J. P. 1992, Shear-wave velocity estimation in porous rocks: Theorical formulation, preliminary verification, and application: Geophys. Prosp., 40, 195-209.

Han, D., Nur, A and Morgan, D.,1986, Effect og porosity and clay content on wave velocity in sandstones. Geophysics, 51, 2093-2107.

Lira, J.E., Vasquez, G, Dillon, L., Bastos, A., Soares, J. 1997, Métodos para geração de perfis de onda S: uma análise crítica a partir da correlação rocha-perfil. Anais do 5º Congresso da SBGF, São Paulo.

Wasserman, P. D., 1989, Neural Computing: theory and Practice. Van Nostrand Reinhold Company

## AGRADECIMENTOS

Agradecemos à Petrobras pela permissão de publicar este trabalho, à Raquel Quadros Velloso e José E. M. Lira pelos comentários e sugestões e a Valdete Barbosa pelo auxílio na edição das figuras.

# Rock Physics of Pore Pressure

*Jack Dvorkin, Stanford University, USA and Ali Mese, Halliburton, USA*

**Abstract**

In gas-saturated sediments, the Poisson's ratio (PR) decreases with decreasing differential pressure (confining minus pore pressure). In liquid-saturated sediments the opposite is true: PR increases with decreasing differential pressure. This means that in gas-saturated sediments, PR decreases with increasing pore pressure and in liquid-saturated sediments it increases with increasing pore pressure. This effect can be used as a new tool for seismic pore pressure and pore fluid monitoring during production as well as for overpressure detection from AVO and elastic impedance inversion, as well as from cross-well, sonic logs and measurements ahead of the drill bit.

## Introduction

Typically, elastic-wave velocity in gas-saturated rock is measured in the laboratory by varying confining pressure while maintaining constant pore pressure. Because velocity reacts to the differential (confining minus pore) pressure, such data can be used to predict in-situ velocity variations in rock with gas due to pore pressure changes at constant overburden. Velocity at in-situ saturation can be calculated from the rock-with-gas velocity via Gassmann's (1951) fluid substitution. Therefore, velocity-versus-pressure data combined with fluid substitution can be used to predict rock elastic property changes in reservoirs during production (Figure 1). Also, these data are a basis for interpreting seismic measurements for pore pressure and fluid variation in time and space.

The time scale of laboratory experiments is much smaller than the geologic time scale of overpressure development. Still, the laboratory experiments where pressure changes rapidly can be used to model the important transient (late-stage) overpressure mechanisms that are invoked when the pressure of the fluid in the rock mass is allowed to increase relative to hydrostatic through (a) aquathermal fluid expansion; (b) hydrocarbon source maturation and fluid expulsion; (c) clay diagenesis; (d) fluid pumping from deeper pressured intervals; and (e) decrease in overburden due to tectonic activity (Huffman, 1998).

The decrease in *Vp* with increasing pore pressure has been used for overpressure detection and production monitoring (e.g., Moos and Zwart, 1998). Yet, velocity does not uniquely define pore pressure because it also depends, among other factors, on porosity, mineralogy, and texture of rock.

We propose to resolve this non-uniqueness and improve the reliability of pore pressure detection by using PR calculated from the P- and S-wave velocity as an overpressure indicator. A combination of PR (often referred to as the elastic impedance) and the acoustic impedance (the product of the P-wave velocity and bulk density) allows one to determine both pore pressure and pore fluid (Figure 2).

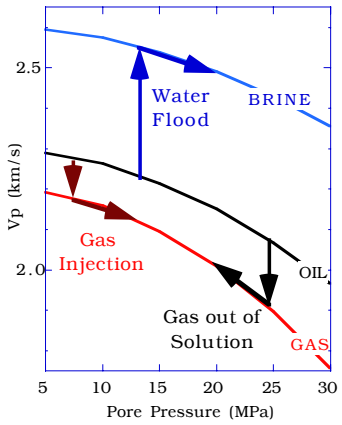


Figure 1 - Laboratory velocity data for a sand sample. Velocity versus pore pressure for 30 MPa confining pressure. Arrows show velocity variation during three different production scenarios. For example, during gas injection, oil is replaced by gas and pore pressure increases; during water flood, oil is replaced by water and pore pressure increases; during gas-out-of-solution drive, oil is replaced by gas and pore pressure decreases.

## Poisson's Ratio and Pressure in Rocks with Gas

PR ($\nu$) can be calculated from the compressional- and shear-wave velocity (*Vp* and *Vs*, respectively) as

$$\nu = 0.5(Vp^2 / Vs^2 - 2) / (Vp^2 / Vs^2 - 1).$$

Nur (1969) was probably first to record the decrease of PR with decreasing differential pressure in room-dry granite and dolomite samples. Nur and Wang (1989) state that the *Vp/Vs* ratio in gas-saturated rocks increases with increasing differential pressure. Wang (1997) supports this statement by laboratory velocity measurements in carbonate samples. This effect appears to be general and can be observed in many sandstone and sand samples. Data from some of them are given in Figure 3 where the porosity range is between zero and 40% and the clay

content range is between zero and 45%. The compressional-wave velocity varies significantly among these samples but PR invariably decreases with increasing pore pressure.

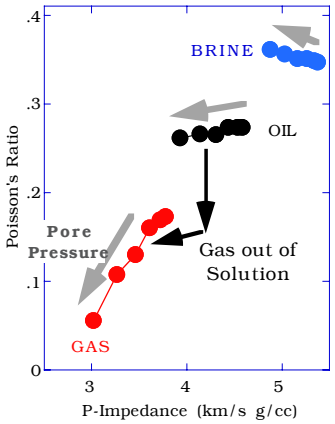


Figure 2 - Poisson's ratio versus P-wave impedance. Bold gray arrows show the direction of pore pressure increase. Only the gas-out-of-solution production scenario is shown.

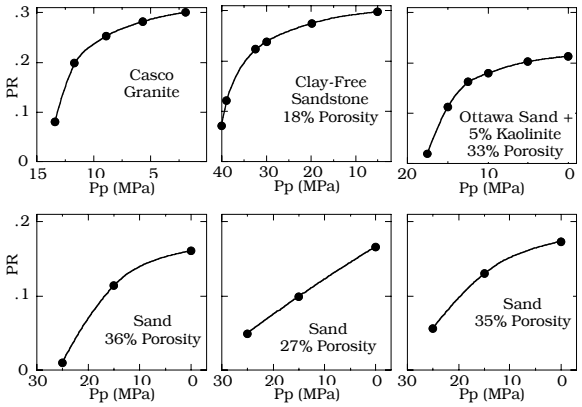


Figure 3 – Gas-saturated rocks. Poisson's ratio (PR) versus pore pressure (Pp) at constant overburden.

Data collected on dozens of sandstone samples are summarized in Figure 4a where the dry-rock PR at normal and high pore pressure is plotted versus porosity. The ranges of the low-pressure and high-pressure PR do not significantly overlap. At the same time, depending on porosity, mineralogy, and texture, the low-pressure velocity in some samples may be in the same range as the high-pressure velocity in others (Figure 4b).

Dvorkin et al. (1999) theoretically explain this PR versus pressure effect as a result of opening of compliant microcracks at increasing pore pressure.

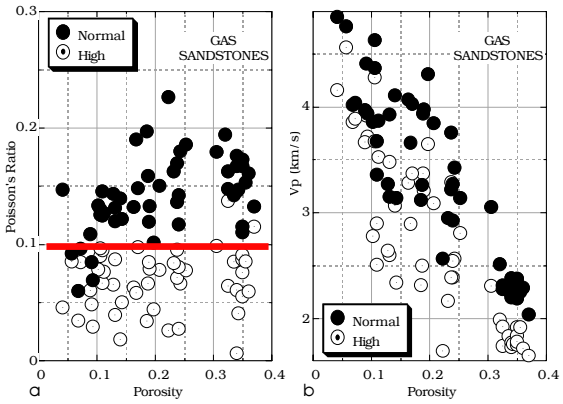


Figure 4 – PR versus porosity and Vp versus porosity in gas-saturated sandstones at high and normal pore pressure. PR values at high pore pressure are distinctively different from those at low pore pressure.

**Poisson's Ratio and Pressure in Rocks with Liquid**

The Poisson's ratio versus pressure behavior in rocks with liquid is opposite to what we observe in rocks with gas. The higher the pore pressure, the softer the rock and the larger the relative increase in the bulk modulus between dry and water-saturated samples. With the shear modulus being the same for the dry and saturated rock (Gassmann, 1951), PR increases with the increasing pore pressure. An example of such behavior is shown in Figure 5 for sand samples.

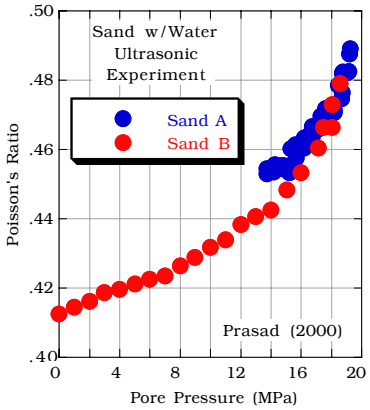


Figure 5 – PR versus pore pressure in two water-saturated sand samples (Prasad, 2000).

The same effect is shown in Figure 6a for a

number of sand samples in a medium-to-high porosity range. In Figure 6b we plot PR at high pore pressure versus Poisson's ratio at normal pore pressure for a suite of gas- and water-saturated sands. The vertical and horizontal axes of this graph have the same scale. PR of water-saturated sand at high pore pressure is larger than that at normal pore pressure while PR of sand with gas at high pore pressure is smaller than that at normal pore pressure.

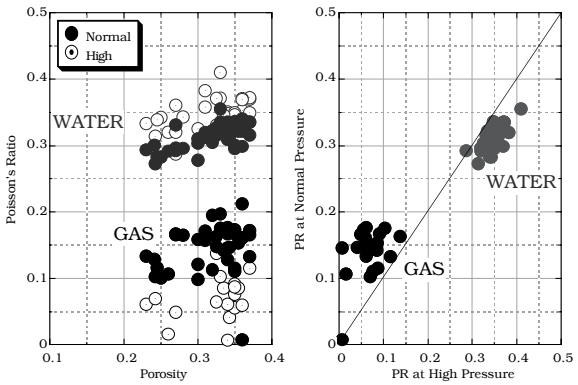


Figure 6 – a. PR versus porosity in sands with gas and water at high and normal pore pressure. The pressure related change in PR is opposite in gas- and water-saturated sands. b. PR at normal pressure versus PR at high pressure in gas- and water-saturated sand.

### Pressure and Fluid Diagnostic Charts

An approximation of Zoeppritz equations states that P-wave reflection $R(\theta)$ at an angle $\theta$ depends on the contrasts of the P-wave impedance $Ip$ and Poisson's ratio $\nu$ at the reflecting interface:

$$R(\theta) \approx R(0)\cos^2\theta + d\left(\frac{1}{1-\nu}\right)\sin^2\theta,$$

where $R(0)$ is the normal reflection:

$$R(0) = \Delta(0.5 \ln Ip),$$

where $\Delta$ is the change across the reflecting interface.

By combining the above two equations, we have:

$$R(\theta) \approx \Delta\left(\frac{\ln I_p}{2}\right) + \Delta\left(\frac{1}{1-\nu} - \frac{\ln I_p}{2}\right)\sin^2\theta.$$

The last equation indicates that it is possible to determine the P-wave impedance from normal seismic reflectivity and Poisson's ratio from reflection at an angle.

Let us explore whether it is possible to identify pore pressure and pore fluid in the Poisson's ratio versus P-wave impedance plane. In Figure 7 we present such cross-plot for sands saturated with water, oil, and gas, and at varying pore pressure. First of all, we can clearly identify the water, oil, and gas domains in this plane. Second, within each domain, we can identify pore pressure following the directions indicated by the arrows.

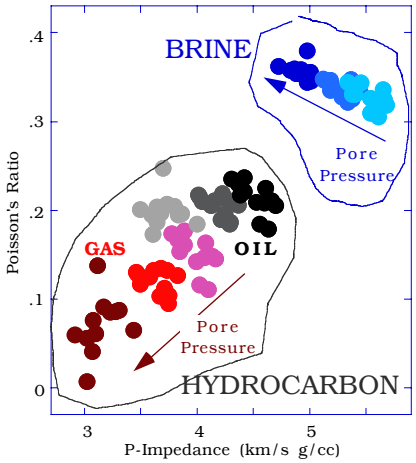


Figure 7 – Pore fluid and pressure diagnostic chart for sands. PR versus *Ip*. Water-saturated sands occupy the top right corner, gas-saturated sands are in the opposite corner, and oil-saturated sands are in the middle. The arrows show pore pressure increase.

### Conclusions

The recent progress of geophysical measurement technology can allow one to extract shear-wave data from surface and marine (bottom cables) reflection profiling, well logs, and cross-well measurements, and, in the future, from measurements ahead of the drill bit.

Because of this, the observed and theoretically confirmed effect of Poisson's ratio decreasing with increasing pore pressure in rocks with gas can be used as a physical basis for a new method of pore pressure and pore fluid monitoring and overpressure detection. This effect was probably implicitly used by Pigott et al. (1990) and Pigott and Tadepalli (1996) in estimating pressure from AVO inversion in carbonates and clastics.

The new method offered here can be used to improve the reliability of traditional methods and their recent modifications (e.g., Bowers, 1994; Moos and Zwart, 1998) where only the compressional-wave

velocity and density or porosity are used and the shear-wave velocity is used to correct for fluid effects.

The effect of pore pressure on the saturated-rock Poisson's ratio can be accurately calculated from the dry-rock data and then used for overpressure prediction as well. Laboratory measurements on representative site-specific rock samples should allow one to quantify and calibrate the observed effects.

Everything said here about Poisson's ratio applies to the *Vp/Vs* ratio as well.

Finally, a pore pressure and fluid diagnostic chart shown in Figure 7 can be displayed in different axes, such as, for example P- and S-wave impedance (Figure 8). Another possibility, commonly used nowadays, is a $\lambda\rho$ versus $\mu\rho$ cross-plot, where $\lambda$ and $\mu$ are the Lame elastic constants, and $\rho$ is the bulk density.

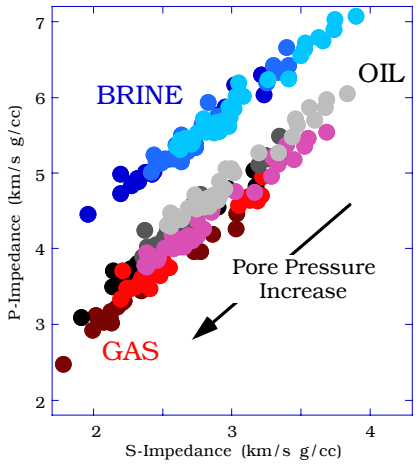


Figure 8 – Pore fluid and pressure diagnostic chart for sands. P-wave impedance versus S-wave impedance. The upper linear trend is for sand with water, the lower trend is for sand with gas, and the middle trend is for sand with oil. The arrow shows pore pressure increase.

**References**

Bowers, G.L., 1994, Pore pressure estimation from velocity data: Accounting for overpressure mechanisms besides under-compaction, IADC/SPE 27488.

Dvorkin, J., Mavko, G., and Nur, A., 1999, Overpressure detection from compressional- and shear-wave data, Geophysical Research Letters, 26, 3417-3420.

Gassmann, F., 1951, Elasticity of porous media: Uber die elastizitat poroser medien, Viertel-jahrsschrift der Naturforschenden Gesselschaft, 96, 1-23.

Huffman, A.R., 1998, The future of pressure prediction using geophysical methods, in Pressure regimes in sedimentary basins and their prediction, Conference proceedings, Houston.

Moos, D., and Zwart, G., 1998, Predicting pore pressure from porosity and velocity, in Pressure regimes in sedimentary basins and their prediction, Conference proceedings, Houston.

Nur, A.M., 1969, Effect of stress and fluid inclusions on wave propagation in rock, Ph.D. Thesis, MIT.

Pigott, J.D., Shrestha, R.K, and Warwick, R.A., 1990, Direct determination of carbonate reservoir porosity and pressure from AVO inversion, SEG 60th Annual Int. Meeting, Extended Abstracts, 2, 1533-1536.

Pigott, J.D., and Tadepalli, S.V., 1996, Direct determination of clastic reservoir porosity and pressure from AVO inversion, SEG 66th Annual Int. Meeting, Extended Abstracts, 2, 1759-1762.

Prasad, M., 2000, Personal communication.

Wang, Z., 1997, Seismic properties of carbonate rocks, in Carbonate Seismology, Palaz, I., and Marfurt, K., eds., SEG Geophysical developments series, 6, 29-52.

Wang, Z., Cates, M.E., and Langan, R.T., 1998, Seismic monitoring of a CO2 flood in a carbonate reservoir: A rock physics study, Geophysics, 63, 1604-1617.

# The effect of in-situ stress on the acoustic transmission response of sandstone rocks.

*Enrique Diego Mercerat†, Kees Wapenaar†, Jacob Fokkema† and Menno Dillen†*

## Abstract

Ultrasonic experiments have revealed an interesting scaling behaviour in the acoustic tranmission response of several sandstone rock samples. The acoustic traces have been recorded for a great variety of ambient pressures that simulate the characteristic in-situ stresses to which reservoir rocks are submitted.

Some assumptions on the micro-structure and mineralogy of the rocks are made. From them, a mathematical model for the pressure-dependent scaling behaviour is derived and tested using numerical modelling techniques. Even simple one-dimensional layered models for wave propagation through the sandstone rocks show scaling behaviour on the transmission response similar to the effect observed in the experimental traces, suggesting our model as a good starting point to analyze the pressure-dependent behaviour of such reservoir rocks.

## Introduction

A couple of years ago, ultrasonic transmission measurements in sandstone rock samples have been carried out at the Laboratory of Rock Mechanics, Department of Applied Earth Sciences, Delft University of Technology. An interesting scaling behaviour of the acoustic transmission response was observed. It appeared that not only the arrival time reduces when the ambient pressure increases, but that the width of the wavelet reduces by approximately the same relative amount. Changes in the amplitude of the seismic signals were also recorded with changing pressure. It seems possible that as a result of changing ambient pressure, some elastodynamic rock parameters will change, causing the observed differences in the arrival time, amplitude and width of the transmitted pulse. The aim of this work is to propose a possible theoretical explanation of the observed phenomena. First, a quick review of the experiments is outlined. After that, the analytical derivation of the scaling model and some numerical results are presented.

†Centre for Technical Geoscience, Department of Applied Earth Sciences, Delft University of Technology, The Netherlands.

## Experimental data

### Pressure machines and acoustic installation

Due to different sample shapes, two pressure machines were used to perform the experiments: the *uni-axial pressure machine* (for prismatic samples) with maximum applied pressure of 20 MPa, and the *tri-axial pressure machine* (only for cubic samples), which pressure range lies between 2 MPa and 82 MPa, in the three perpendicular axial directions. In each pressure plate, three piezoelectric broad-band transducers are mounted, one P-transducer and two mutually perpendicular polarized S-transducers. They have a central frequency of 1 MHz and they are in direct contact with the sample and pressed, by means of a spring, with a constant force on the block.

### Rock samples

Several sandstone rock samples were used in the experiments. They are all rather clean sandstones containing quartz, feldspar and, to a lesser extent, some rock fragments. They represent typical reservoir rocks with a wide range of porosity values (5 % - 20 %). For a detailed mineralogical and petrophysical characterization of the rocks, we refer the reader to Dillen (2000).

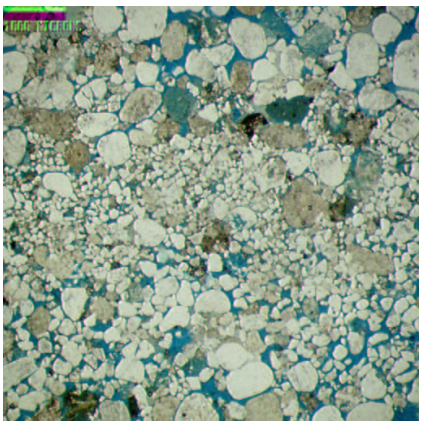

Figure 1: Thin section micro-photograph Rotliegend sandstone

In Figure 1, a micro-photograph of Rotliegend Sandstone can be seen. This thin section comes from a core drilled in a well at the northern Netherlands' off-shore, and it was not used for the ultrasonic experiments. From the matrix structure, it is possible to hypothesize that different grains can react differently to large in-situ stresses. Harder quartz grains may remain unchanged, while softer grains (i.e. feldspar, clay cement) or grain contacts may strongly change their acoustic parameters as a function of applied pressure. Also some reordering of the grains following preferable directions (for example, perpendicular the to main effective stress) can occur.

### Scaling behaviour

Pressure-dependent dynamic characteristics of the sandstone rocks are fully described in Dillen (2000) and Swinnen (1997). In this work, we are specially interested in the scaling behaviour of the transmission response. It is worthwile to mention that the scaling of the traces has been observed in every sandstone sample and both in P and S waves arrivals. Also it has been carefully checked that the time and amplitude changes are not source effects, therefore it is the propagation through the sandstone that changes with changing pressure. In Figure 2, the scaling behaviour in the Rotliegend sandstone can be clearly seen. The time-axis seems to be scaled by a single factor when the ambient pressure is changed from one value to the other. Also the amplitude changes when changing the pressure.

## The binary layered medium approach

In order to study the scaling behaviour analytically, we start by making a number of assumptions: we consider the sandstone horizontally layered. Secondly, the layered medium consists of only two types of material (hence the name binary layered medium), and the third assumption is that changes in the ambient pressure do not affect the layer thicknesses, but only the material acoustic parameters. Figure 3 exemplifies the assumed model for two different pressure states.

With these assumptions the depth-dependent normal-incidence plane-wave reflectivity $r(z)$ obeys the following scaling relation

$$r_B(z) = \beta\, r_A(z), \tag{1}$$

where the subscripts $A$ and $B$ refer to two different ambient pressure states. When the material parameters of both layer types react similarly (in a relative sense) to changes in the ambient pressure then $\beta = 1$; when they react differently, then $\beta \neq 1$. The average vertical slowness $\bar{s}$ of the material obeys the following relation

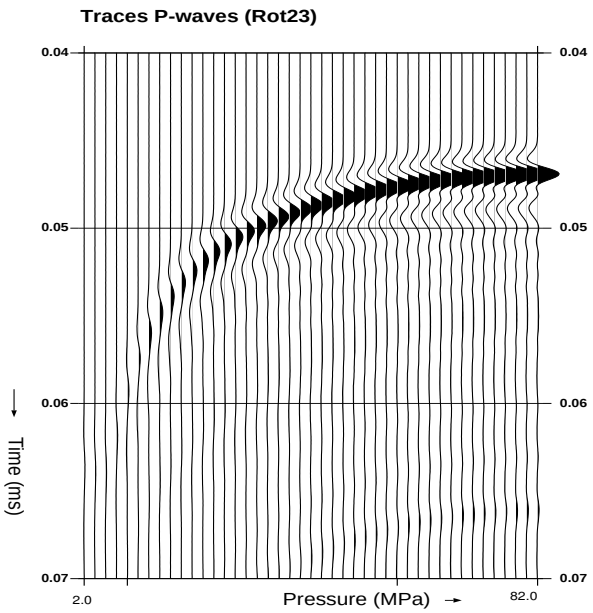


Figure 2: P-waves for increasing pressure (tri-axial pressure machine) in Rotliegend sandstone

$$\bar{s}_B = \alpha\, \bar{s}_A. \tag{2}$$

In the following section we will evaluate the scaling behaviour of the transmission response of binary layered media analytically.

### Scaling behaviour of the transmission response

The normal-incidence plane-wave transmission response of a layered medium can be expressed in the frequency domain in terms of a 'generalized primary' propagator $\mathcal{W}(z_1, z_0, \omega)$, according to

$$\begin{aligned} \mathcal{W}(z_1, z_0, \omega) &= \mathcal{P}(z_1, z_0, \omega)\mathcal{M}(z_1, z_0, \omega) \\ &= \exp\{-j\omega\bar{s}\Delta z\}\exp\{-\mathcal{A}(2\omega\bar{s})\Delta z\}, \end{aligned} \tag{3}$$

where $\Delta z = z_1 - z_0$. The first exponential describes the (flux-normalized) primary propagation from depth level $z_0$ to $z_1$ and the second exponential accounts for the internal multiples generated at all interfaces between those two depth levels. The function $\mathcal{A}$ is the Fourier transform of the 'causal

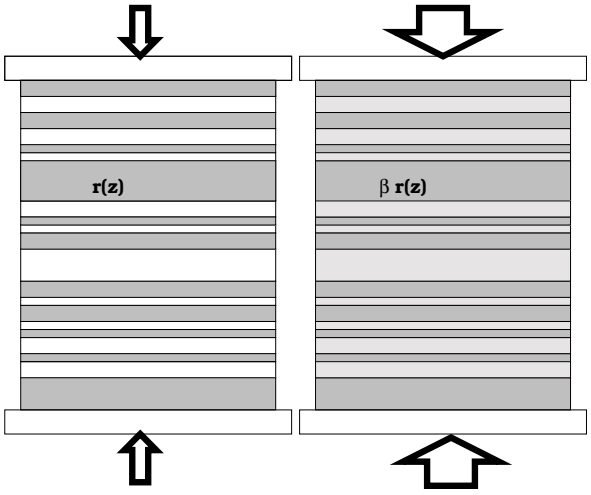


Figure 3: Two different pressure states in a binary layered medium. Left: state A (lower pressure), Right: state B (higher pressure)

part' of $\mathcal{S}(z)$, according to

$$\mathcal{A}(k) = \int_0^\infty \exp\{-jkz\}\mathcal{S}(z)\mathrm{d}z, \qquad (4)$$

where $\mathcal{S}(z)$ is the autocorrelation of the reflection function $r(z)$, expressed by,

$$\mathcal{S}(z) = \frac{1}{\Delta z - z}\int_{z_0}^{z_1 - z} r(\zeta)r(\zeta + z)\mathrm{d}\zeta. \qquad (5)$$

Note that equation (3) is the well-known O'Doherty-Anstey relation (O'Doherty and Anstey, 1971), except that $\mathcal{A}(k)$ in equation (4) is expressed in terms of a spatial rather than a temporal autocorrelation function. The depth-time conversion takes place in equation (3), where $\mathcal{A}(k)$ is evaluated at $k = 2\omega\bar{s}$. Assuming $r(z)$ obeys equation (1), $\mathcal{A}(k)$ has the following scaling behaviour

$$\mathcal{A}_B(k) = \beta^2\,\mathcal{A}_A(k), \qquad (6)$$

where the subscripts $A$ and $B$ refer again to two different ambient pressure states. For these two pressure states the generalized primary propagators read

$$\begin{aligned}\mathcal{W}_A(z_1, z_0, \omega) &= \mathcal{P}_A(z_1, z_0, \omega)\mathcal{M}_A(z_1, z_0, \omega) \qquad (7)\\ &= \exp\{-j\omega\bar{s}_A\Delta z\}\exp\{-\mathcal{A}_A(2\omega\bar{s}_A)\Delta z\},\end{aligned}$$

$$\begin{aligned}\mathcal{W}_B(z_1, z_0, \omega) &= \mathcal{P}_B(z_1, z_0, \omega)\mathcal{M}_B(z_1, z_0, \omega) \qquad (8)\\ &= \exp\{-j\omega\bar{s}_B\Delta z\}\exp\{-\mathcal{A}_B(2\omega\bar{s}_B)\Delta z\},\end{aligned}$$

or, using equations (2) and (6),

$$\begin{aligned}\mathcal{W}_B(z_1, z_0, \omega) &= \exp\{-j\alpha\omega\bar{s}_A\Delta z\}\exp\{-\beta^2\mathcal{A}_A(2\alpha\omega\bar{s}_A)\Delta z\}\\ &= \mathcal{P}_A(z_1, z_0, \alpha\omega)[\mathcal{M}_A(z_1, z_0, \alpha\omega)]^{\beta^2}. \qquad (9)\end{aligned}$$

## Numerical simulation

In order to test the scaling behaviour expressed by equation (9), we have performed numerical simulations for the transmission response through a binary layered medium. The total transmission response is calculated by means of forward modelling of the acoustic wave equation in the frequency domain, considering a plane-wave incident from the top and calculating the plane-wave transmitted to the bottom of the stack of horizontal parallel layers. After calculating the transmission impulse response, convolution with a Ricker wavelet is carried out.

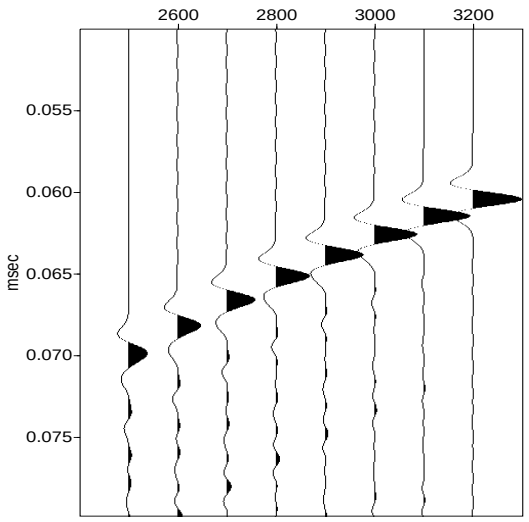


Figure 4: Transmission responses for binary layered media. Velocity of material 1 = 3500 m/s. Velocity of material 2 is labeled in the horizontal axis

In Figure 4, transmitted zero-phase Ricker wavelets through binary layered media are shown. The rightmost trace corresponds to the smallest impedance contrast and average slowness [†]. The other traces are calculated by fixing one velocity and decreasing the other, that is increasing the impedance contrast and the average slowness of the models. Note that the scaling behaviour in Fig-

[†]In all simulations, the density of the stack of layers is considered constant

ure 4 is similar to that observed in the experimental data for different ambient pressures (Figure 2). The first, third and fifth traces from the right are used to check equation (9). The direct path delay is subtracted from both responses according to the corresponding time delay for each model calculated via forward modelling. Thus equation (9) simplifies to

$$\mathcal{M}_B(z_1, z_0, \omega) = [\mathcal{M}_A(z_1, z_0, \alpha\omega)]^{\beta^2}. \qquad (10)$$

From the model velocities and using equations (1) and (2), it is possible to calculate the scaling parameters $\alpha$ and $\beta$ to scale the fastest transmission response (3500 - 3200 m/s) to the next arrivals (3500 - 3000 m/s and 3500 - 2800 m/s) in Figure 5.

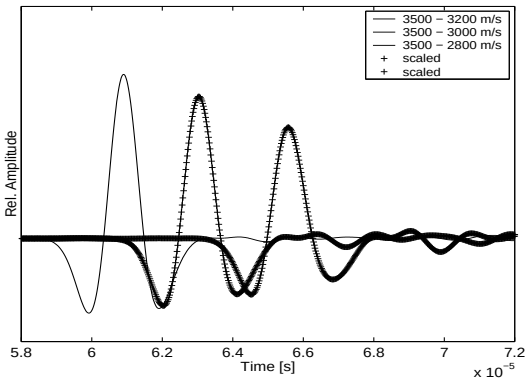


Figure 5: Detail of the first, third and fifth traces (from the right) of Figure 4 and scaled versions from the fastest arrival to the other two using equation (9).

As follows from the latter formulation, the scaling model must be applied to the transmission impulse response, that is, with no source function included. As a first step in our forward modelling algorithm, the plane-wave transmission response through the stack of layers is calculated. Then the scaling relation (equation (10)) is applied. Finally, the transmission impulse responses are convolved with a Ricker wavelet and shifted back to the correct arrival time. In Figure 5 the results are displayed. The match between the scaled versions and the calculated transmission responses is almost exact. This is another numerical confirmation of the O'Doherty-Anstey relation, although we know it is only an approximation to the total transmission response through a layered sequence.

# Discussion and conclusions

The attenuation and dispersion of seismic energy due to superposition of internal multiples may well be the cause of the scaling of the transmitted wavelets through a rock sample under varying ambient pressure. The wavelet scaling produced by changes in the impedance contrast between layers corresponds to the pressure-dependent scaling behaviour observed in the experimental data. This correspondance suggests that as the ambient pressure increases, the average slowness and the impedance contrast within the rock decrease.

Equation (9) quantifies the scaling behaviour of the transmission response. The $\alpha$ parameter acts on both the arrival time and the width of the wavelet when the ambient pressure is changed. The exponent $\beta^2$ in the second term accounts for the amplitude change, but has an effect on the phase as well. Since this exponent is applied to a frequency-dependent term, there is not a simple scaling relation in the time-domain.

Although we have made a number of simplifying assumptions, it is worthwhile to use equation (9) as a first approximate model for observations like those in Figure 2. The $\alpha$ and $\beta$ parameters are directly related with acoustic characteristics of the layered model (i.e. reflectivity and average slowness). Estimating them from that type of measurements for a range of different ambient pressures gives valuable information about the pressure-dependent behaviour of the reservoir rock. However, more realistic 3-D scattering models within the rock matrix may also present the scaling behaviour of the transmission response. Present research is focused on that direction.

# References

Dillen, M. W. P. *Time-lapse seismic monitoring of subsurface stress dynamics*. PhD thesis, Delft University of Technology, 2000.

O'Doherty, R. F. and Anstey, N. A. Reflections on amplitudes. *Geophysical Prospecting*, 19:430-458, 1971.

Swinnen, G. The effect of stress on wave propagation in reservoir rocks. Master's thesis, Katholieke Universiteit Leuven, Department of Civil Engineering, 1997.

# Theoretical Model for the Geo-electrical Response of Fresh Water Shaly Sandstones

*Olivar A. L. de Lima, Michael B. Clennell and Sri Niwas, CPGG/UFBA*

**Abstract**

The electrical behavior of a shaly sandstone aquifer saturated with freshwater is analyzed based on the volume-conductivity approach proposed by Lima and Sharma (1990; 1992). Such an approach has been shown to be satisfactory to describe both laboratory and well log data under saline water saturation. Here we shown that the electrical behavior and the convex-upward curvature of a plot of the bulk conductivity against the electrolyte conductivity reflect not only the textural and clay mineralogic effects, but also those due to the salinity of its pore electrolyte. Analytical expressions are written both for the conductivity of the aquifer and of their constituent elements. They are written in a form that emphasize the conductive behavior of shaly and clean sandstones, with fresh pore fluid, as demonstrated by several experimental laboratory data.

**Introduction**

The electrical conductivity is one of the most important physical properties from which we can evaluate the hydrological characteristics of reservoir rocks. For shaly sandstones several empirical relations based on statistical treatments of experimental observations and/or analytically supported by sound physical principles have been proposed in the literature (Waxman & Smits, 1968; Clavier et al., 1984; Worthington, 1985; Sen et al., 1988; Lima and Sharma, 1990, Revil and Glover, 1997). Under saline water reservoir saturations most of these formulas reduce to the linear relation

$$\sigma_0 = \frac{A}{F}\left[\sigma_w + \Sigma_S\right] \quad , \qquad (1)$$

with $A$ as a non-dimensional geometrical parameter and $\Sigma_s$ a constant measuring the conductive contribution added by clays or shaly materials. In fact, $\Sigma_s$ is a combination of shape factors of the pore space and of an electric parameter describing the macroscopic effects of the ionic double layers around the clay platelets.

For a fresh water reservoir, however, even the simple Archie's formula (Archie, 1942) appears to fail in its application (Alger and Harrison, 1989; Glover et al., 2000). This mainly results from the fact that under freshwater conditions, the current paths through the medium do not behave as simple parallel resistors arrangement. In addition, at low salt concentration, $\Sigma_s$ may be also controlled by the electrolyte conductivity. This may explain the restricted use, and sometimes the discrepant results found in the log interpretation of groundwater wells, and even in oil well of fresh water environments (Blenkinsop et al., 1986, Savena and Sibbit, 1990).

In this paper, based on the grain conductive model of Bussian (1983) and Lima and Sharma (1990; 1992) we develop a new scheme to describe the conductive behavior of clays, shales and shaly sandstones under fresh water saturation. This analytical scheme has been tested with theoretical models and different sets of laboratory data from several sources.

**Experimental Evidence**

Experimental laboratory results for shaly sandstones show that a plot of $\sigma_o$ versus $\sigma_w$ are smooth curves having linear trends as $\sigma_w \to \infty$. At low $\sigma_w$, however, they shown a non-linear behavior reflecting the fact that the electrical tortuosities through the wet clay material and that in the free pore channels are quite dissimilar and intricately connected (Sen et al., 1988; Lima and Sharma (1992; Revil and Glover, 1998). The conductive contributions associated with the clays in the matrices are almost constant and become most noticeable at low $\sigma_w$. Surface conduction may even increase at low $\sigma_w$, due to an increase in the counterion mobility within the double layers. These features are well depicted in a log-log plot of the experimental data (Figure 1). Such behavior also support the experimental evidence that the flow of a fluid in such rocks is more closely related to its electrolyte conduction than to that within their shaly matrices.

For shales we also observe similar influences. Figure 2 is a plot of $\sigma_{sh}$ versus $\phi_{sh}$ for artificial shales made with waters of different salinities. We observe linear trends for high porosities, of positive inclination at high $\sigma_w$ and negative ones at low $\sigma_w$. In both case, we see a non-linear behavior at low $\phi_{sh}$.

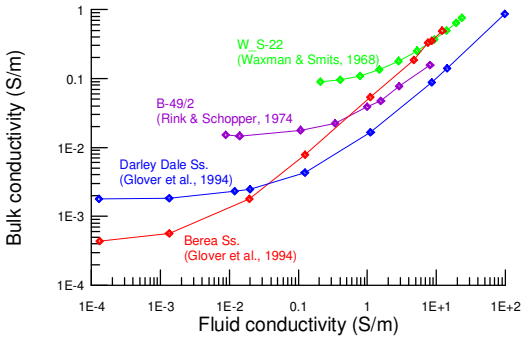


***Figure 1*** *- $\sigma_o$ - $\sigma_w$ plot for different shaly sandstones laboratory data.*

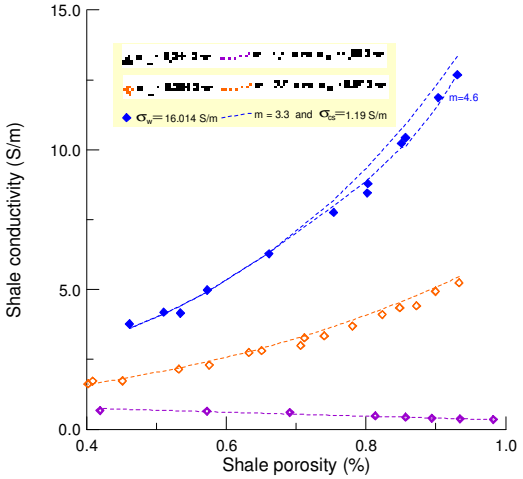


***Figure 2*** *- $\sigma_o$ - $\sigma_w$ plot for artificial shales is the different waters (data from Cremers and Landelout, 1966).*

## Theoretical Developments

The volume conductivity approach, originally proposed by Bussian (1983) and extended by Lima and Sharma, (1990; 1992) is physically consistent with the general behavior described above. This approach has the great advantage of circumventing the need for a explicit microscopic treatment of the electrical conduction through charged particles. It express the conductivity of a shale or shaly sandstone by means of the self-similar Buggeman relation as

$$\sigma_0 = \frac{\sigma_w}{F}\left(\frac{1-\sigma_{cs}/\sigma_w}{1-\sigma_{cs}/\sigma_0}\right)^m \qquad (1)$$

$$= \frac{\sigma_w}{f}\left(\frac{1-\sigma_w/\sigma_{cs}}{1-\sigma_0/\sigma_{cs}}\right)^{m_c} ,$$

where $F = \phi_e^{-m} = f^{m-1}$, is the intrinsic formation factor, $m_c = m/(m-1)$, $m$ being a non-dimensional parameter that depends on the aspect ratio of the grains and of their topological distribution, $\sigma_{cs}$ is the equivalent condictivity of the solid matrix grain, and $\sigma_w$ is the conductivity of the host fluid filling the interconnected porosity of the medium. When $\sigma_{cs} = \sigma_w$ equation (1) predicts an iso-conductivity point where $\sigma_0 = \sigma_{cs}$. In figures 2 and 3 the curves are computed according to equation (1), after a best fit determination of $\sigma_{cs}$ and $m$ using equation (2). Parameter $m$ (or $m_c$) has a strong influence on the tortuosities of the main conducting paths throughout the medium.

Equation (1) reproduces Archie's equation when $\sigma_{cs} = 0$, and has a Waxman – Smits (W-S) or a dual-water (D-W) equivalent expression when $\sigma_w >> \sigma_{cs}$ (Lima and Sharma, 1990). It can even be simplified to an Archie – Winsauer version by making

$$a = \left(\frac{1-\sigma_{cs}/\sigma_0}{1-\sigma_{cs}/\sigma_w}\right)^m ,$$

$a$ being a function of $\sigma_w$, $\sigma_{cs}$ and $m$, that tends to 1 as $\sigma_{cs} \rightarrow 0$. For a given sample, and within a certain range of water resistivities, $a$ may be taken as approximately constant. This offers a physical justification and a mathematical explanation for the modified Archie-Winsawer empirical equation (Winsauer et al., 1952).

Introducing the apparent formation factor defined as $F_a = \sigma_w/\sigma_o$, equation (1) can be rewritten as

$$\frac{\sigma_{cs}}{\sigma_w} = \frac{1-(F/F_a)^{1/m}}{1-F_a(F/F_a)^{1/m}} \quad . \qquad (2)$$

Equation (2) has a form appropriate for use in quantitative log interpretation. It should be applied twice: (i) one for the virgin condition where the rock is completly filled with water of conductivity $\sigma_w$ ($F_a^{(1)} = \sigma_w/\sigma_o$ , $\sigma_o$ being the reading of a deep logging tool); another for the invaded zone with a mud filtrate of conductivity $\sigma_{mf}$ ($F_a^{(2)} = \sigma_{mf}/\sigma_{xo}$ , $\sigma_{xo}$ being the reading of a shallow logging tool). Thus, knowing $\phi_e$, we can

solve equation (2) iteratively to find $m$ and $\sigma_{cs}$ along the depth of the well.

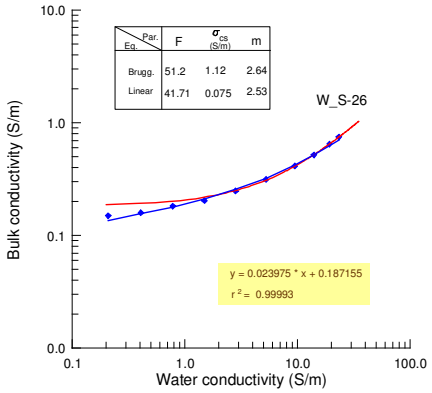


***Figure 3*** - *$\sigma_o$ - $\sigma_w$ plot for a shale sandstones sample. (data from Waxman and Smits, 1968).*

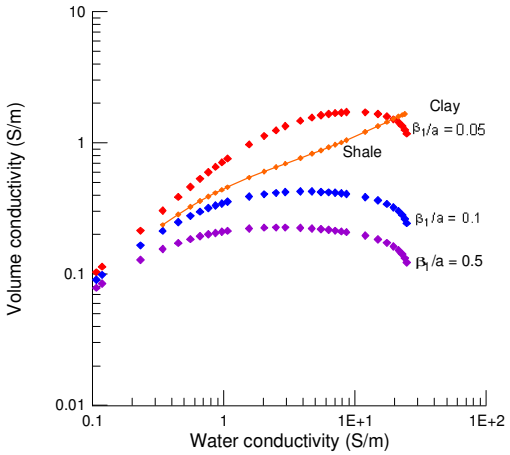


***Figure 4*** - *$\sigma_o$ - $\sigma_w$ simulation plot for clays and shale using Lima and Sharma (1992) model.*

Evidently equation (1) or (2) can also be applied to pure shales (see fig. 2). In such cases $\sigma_{cs}$ will be the conductivity of a wet clay particle (including its bound water), and $\phi_{sh}$ measures the micro pore space filled with the additional water to complete saturation. For a clay coating structure of a representative shaly sand particle, taken as a sphere, we can use the following equation (Lima and Sharma, 1990)

$$\sigma_{cs} = \frac{2p\,\sigma_{sh}}{3-p}\ ,$$

to compute the shaly volume fraction $p$ in the composed sandstone matrix. In terms of the sample volume this fraction is given as $v_{cl} = (1-\phi_e)p$.

In Figure 3 we shown the best fit solution obtained with equation (2) for the shaly sandstone sample C-26 analysed by Waxman and Smits (1968). We note that taking only the points falling in the linear portion, we find $\sigma_{cs}$ and $m$ that are very close to the ones obtained by a straight line fit to the same points. However, using only the data points of the non-linear portion, $\sigma_{cs}$ and $m$ are found to be greater than the previous ones by more than 20%. A similar result has been observed also with the shale data of figure 2.

For a wet clay particle Lima and Sharma proposed the following conductivity function

$$\sigma_c = \frac{2\delta_1\sigma_w}{2+\delta_1}\ , \qquad (3)$$

where $\delta_1 = \beta_1/aC_1$, $\beta_1$ is the surface counter-ion density necessary to balance the immobile charges on a clay particle of radius $a$, and $C_1$ is the ionic concentration in the electrolyte. Figure 4 show the theoretical conductive response for representative clay particles using three different values of $\beta_1/a$. We also compute a theoretical shale response based on equation (1), for $\beta_1/a = 0,1$ with $F = 20$ and $m=2$. Note the non-linear behavior at low $\sigma_w$ and the constant plateau for $\sigma_c$. At very low or very high $\sigma_w$ the equation (3) may not apply (Lima and Sharma, 1992). The simulated shale depict the general behavior observed with experimental data.

## Conclusion

In the present work we review and extended the macroscopic, grain conductivity approach for shaly and shaly sandstones, as proposed by Lima and Sharma (1990). In particular, we examine the behavior of the pertinent equations in the low salinity region, in which $\sigma_w < \sigma_{cs}$ . We find that under fresh water saturation the exponent $m$ may increase with respect to $m$ found in the high salinity linear regime.

## References

Alger, R.P. and Harrison, C.W., 1989, Improved fresh water assessment in sand aquifers

utilizing geophysical well logs. The Analyst, 30, 31-44.

Archie, G.E., 1942, The electrical resistivity log as an aid in determining some reservoir characteristics: Trans. AIME, 146, 54-62.

Blenkinsop, M., Baker, P., Clavier, C., Kenyion W. and Des Ligneris, S., 1986, Deep electromagnetic propagation tool interpretation. SPWLA, Long. Sym. Paper XX.

Bussian, A.E., 1983, Electrical conductance in a porous medium. Geophysics, 48, 1258-1268.

Clavier, C., Coates, G. and Dumanoir, J., 1977, Theoretical and experimental bases for the dual water model for the interpretation of shaly sands. Soc. Petr. Eng. J., 4, 153-168.

Cremers, A.E. and Landelout, H.., 1966, Surface mobiles of cation in clays. Proc. Soil Sci. Soc. An., 30, 570-576.

Glover, P.W.J., Hole, M.J. and Pous, J., 2000, A modified Archie's low for two conducting phases, Earth and Planet. Sci. Let., 180, 369-383.

Lima, O.A.L. and Sharma, M.M., 1990, A grain conductivity approach to shaly sandstones. Geophysics, 55(10).

Lima, O.A.L. and Sharma, M.M., 1992, A generalized Maxwell-Wagner theory for membrane polarization in shaly sands. Geophysics, 57, 431-440.

ionic-surface electrical conduction in porous media. Phys. Rev. B 55, 1757-1773.

Revil, A., Glover, P.W.J., 1998, Nature of surface electrical conductivity in natural sands, sandstones, and clay. geophys. Res. Let. 25, 691-694.

Saxena, V. and Sibbit, A.M., 1990, Deep saturation in low salinity reservoirs from dual laterolog quadrature signals. Soc. petr. Eng. Tech. Conf., Paper 20560.

Sen, P.N., Goode, P.A. and Sibbit, A., 1988, Electrical conduction in clay bearing sandstones at low and high salinities. J. Appl. Phys., 63, 4832-4840.

Waxman, M.H. and Smits, L.J.M., 1968, Electrical conductivities in oil-beaving shaly sands. Soc. Petr. Eng. J., 8, 107-122.

Whorthington, P.F., 1985, The evolution of shaly sand concepts in reservoir evaluation. The Log Analyst 26, 23-40.

Winsauer, W.O. Shearin Jr., H.M., Masson, P.H. and Williams, .M., 1952, Resistivity of brine – saturated sands in relation to pore geometry. An. Ass. Petrol. Geol. Bull. 36, 253-277.

**Acknowledgments**

This work is part of a cooperative research project between CPGG/UFBA and CENPES/PETROBRAS, financed by the FINEP/CTPETRO/UFBA/FAPEX, convenium # 65990473.00.

# Velocity Dispersion and Attenuation in Brazilian Sandstones

*Guilherme Fernandes Vasquez*, PETROBRAS, Ivan de Araújo Simões Filho, UNICAMP, Lúcia Duarte Dillon, PETROBRAS, and Carlos Henrique Lima Bruhn, PETROBRAS.*

**Summary**

It is well known that attenuation data should be a very powerful tool to rock and fluid type determination. Attenuation properties are sensitive to rock and fluid type, partial saturation, presence of cracks and other parameters which are difficult to obtin by the conventional seismic method. Nevertheless, seismic wave attenuation studies are very rare compared to seismic wave velocities and its relationships to rock properties, in part due to the theoretical and experimental difficulties involved. Laboratory measurements of attenuation under well-controlled conditions are useful to gain qualitative insights on the wave propagation process and its relationships with rock and fluid properties. In this paper we present some results on the study of seismic attenuation of Brazilian rocks.

**Introduction**

Measurement and understanding of seismic attenuation are difficult tasks. It's well known that this phenomenon is related to rock and fluid properties, but some examples in the literature shows distinct or even conflicting results. More laboratory studies, under well-controlled conditions, are needed. Although quantitative results may not be extendable to field data due to the differences in frequency content of the experiments, laboratory data gives important insights and information of the qualitative behavior of attenuation.

We report here studies on the behavior of the compressional and shear waves velocities and quality factors in three different Brazilian reservoirs (one turbidity offshore sandstone deposit from Campos Basin, and two fluvial and eolic reservoirs, one from Reconcavo Basin and other from Potiguar Basin) and its relationships with facies attributes.

This study is based on ultra-sonic pulse propagation laboratory experiments in dry, brine and oil saturated rocks and permeability, porosity and petrographic analysis information. The results were interpreted based on the global flow (Biot's theory) and local fluid flow models, and the real data was compared to theoretical predictions. We found that the viscoelastic behavior are somewhat correlated with the particular diagenetic history of each reservoir sandstone. Among the observed correlations stands out the fact that the compressional and shear wave velocities are strongly dependent upon the porosity, cementation degree and clay content, while the quality factors are more influenced by the cementation, total pore fill and porosity.

**Method**

Compressional and shear wave velocities ($V$p, $V$s) and quality factors ($Q$p, $Q$s) were measured in 73 room-dry samples. From this set of samples, 40 were brine saturated and 12 oil saturated. Velocity measurements were made by ultrasonic transmission technique at 500kHz. Quality factors (related to attenuation) were measured by the spectral ratio method well described in Toksöz *et al*. (1979).

The brine and oil saturated velocities results were compared to the predictions of the high-frequency limit of the Biot theory (Biot, 1956) and, when possible, with the Mavko and Jizba (1991) local fluid flow approximation. These predictions uses dry rock elastic properties, measured at the laboratory, and fluid elastic properties, calculated as proposed by Batzle and Wang (1992).

**Results**

Both P and S wave attenuation rises when changing from room-dry to saturated condition, the changes being greater for oil saturated samples. These features suggest the importance of pore fluid viscosity. For brine saturated samples the change in attenuation from dry to saturated conditions are unrelated to permeability, but it seems that for oil saturated samples the increase in attenuation are smaller for higher permeabilities. Figure 1 presents an example of the behavior of the quality factor with pressure for the same sample dry, brine, and oil saturated.

We can define the apparent dispersion as the percent difference between the measured velocity and the Gassmann (or Biot low frequency limit) predicted velocity:

$$\text{Apparent Dispersion} = (V_M - V_G)/V_G .$$

We can also define the Biot dispersion as the percent difference between the velocity prediction for high and low frequency limits from Biot theory:

$$\text{Biot Dispersion} = (V_B - V_G)/V_G .$$

Where $V_M$ is the velocity measured in the lab, $V_G$ is the Gassmann calculated rock velocity and $V_B$ is the high frequency limit for the velocity. The apparent P wave dispersion of brine saturated samples tends to decrease as permeability increases, as shown in figure 2 for the turbiditic reservoir data set. The Biot dispersion shows the opposite behavior, increasing with

permeability. This feature was also observed by Wang and Nur (1990).

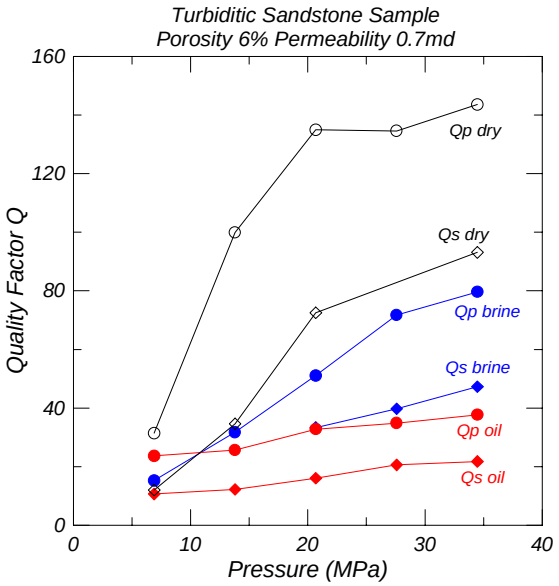


Figure 1 - Quality factor versus pressure for one turbiditic sample dry, brine and oil saturated.

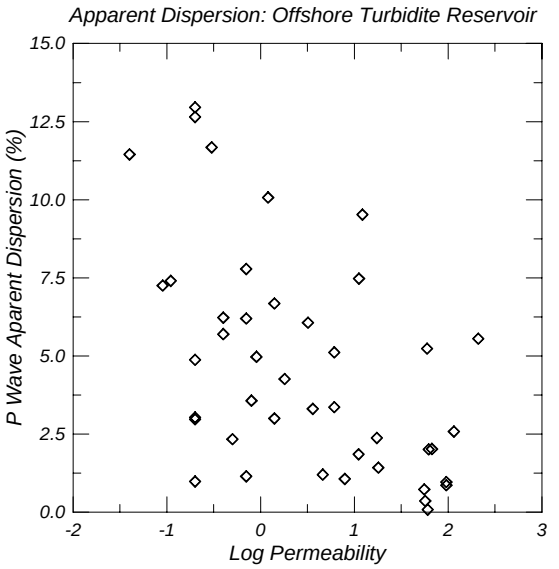


Figure 2 - Apparent dispersion versus permeability for brine saturated samples.

The total quality factor and velocity increment as we move from low (ambient) to high (34.5MPa) pressure tends to increase with increasing permeability. This may result from the closure of micro-cracks and grain contacts, preventing local fluid flow into the pore space at some extend.

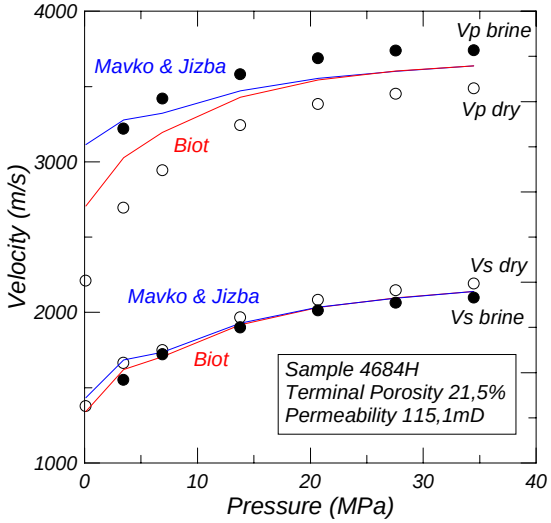


Figure 3 – P and S-wave velocities measured and predicted based on Biot and Mavko & Jizba.

Biot predictions works fairly well in some cases, but the Mavko and Jizba predictions gives much better results, particularly when it involves viscous fluid (oil). Velocity estimations by the Biot high frequency limit fail with high viscosity fluids because the local flow becomes still more prominent. Figure 3 illustrate the comparison of velocities measured on a brine-saturated sample and the Biot and Mavko & Jizba predictions.

At the reservoir scale the studied turbiditic sandstone presents relatively well distributed clay content, generally less than 20%, but the calcite cementations are heterogeneous and can reach values up to 58%. Calcite concretions may be nodes of few centimeters or even patches with some meters dimensions. The velocity and quality factor of this sandstone increases as the calcite content increases and decreases as the clay content increases.

The procedure proposed by Blangy *et al* (1993) to predict reservoir quality can be used to illustrate the role of calcite on rock elastic properties, as shown in Figure 4. Plotting the bulk modulus of the samples against its porosity a linear fit can be drawn cutting the porosity axis at the critical porosity values and the moduli axis at the solid fraction bulk modulus. Also, lines can be drawn crossing the moduli axis at the values corresponding to clay, quartz and calcite moduli and the porosity axis at the critical porosity point. We observe that samples with more than 10% calcite tends to lie between quartz and calcite lines.

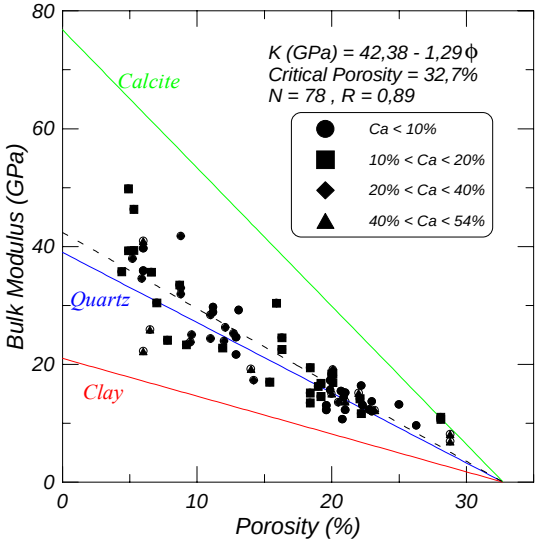


Figure 4 - Bulk Modulus against porosity with lines for clay, quartz and calcite.

The velocity-porosity relation can be well described by linear laws, as in so many examples reported worldwide. Quality factors are poorly related to porosity, but with an evident trend of decreasing quality factor with increasing porosity. One may consider that the porosity is related to frame stiffness so, even it doesn't affects attenuation directly, there's some indirect influence.

Velocity and permeability presents a quite good relation which can be approximated by a linear regression between velocity and permeability logarithm, as illustrated on figure 5 for brine-saturated samples from the turbiditic sandstone data set. Linear regressions involving velocity, porosity and (log) permeability has correlation coefficients of the order of 0.9. Dry and brine saturated rocks quality factors decreases with permeability in a similar fashion to velocity, but oil-saturated samples tends to present higher $Q$ for larger permeabilities. The quality factor of brine saturated turbiditic sandstones are plotted against permeability in figure 6.

At one hand, after Biot, the characteristic frequency, $\omega_c$ (roughly, the boundary between high and low range) is given by:

$$\omega_c = \eta\phi / k\,\rho.$$

where $\phi$ is porosity, k is permeability, $\rho$ is fluid density. And $\eta$ it's viscosity. On the other hand, squirt-flow mechanisms lead to:

$$\omega_c = K\alpha^3 / \eta.$$

Most measurements were made under room temperature. Varying the temperature form 25ºC to 100ºC we observed that velocities and quality factors decrease with increasing temperature. The velocity decrease can be explained by Biot or local flow models, as it is related mainly to the fluid modulus reduction. The Quality factor increase (or attenuation decrease) is an evidence of the local flow mechanism and it's related to the fluid viscosity reduction.

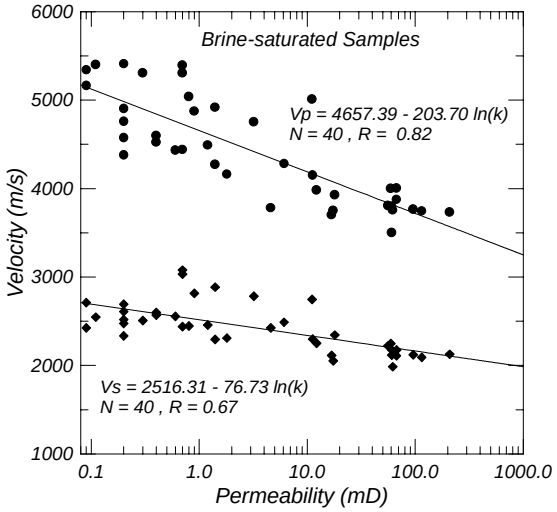


Figure 5 - Velocity-permeability relation for brine saturated samples.

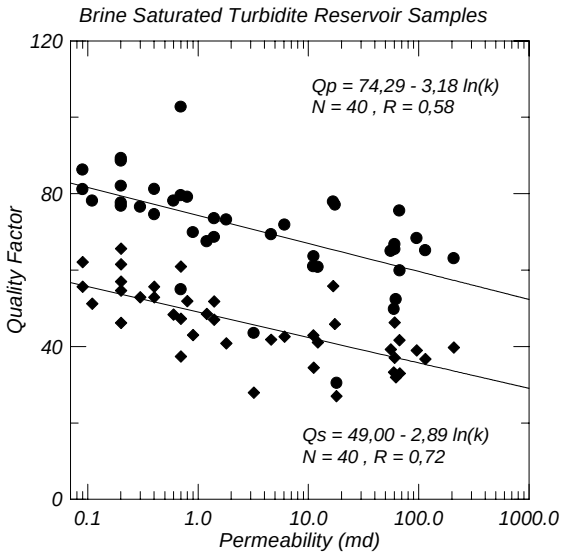


Figure 6 – Quality factor versus permeability.

Figure 7 shows the apparent dispersion for fluvial sandstone samples as a function of temperature, all samples are oil saturated. While the apparent dispersion decreases as temperature increases, the Biot dispersion are almost constant. Figure 8 shows the compressional-wave quality factor of turbiditic sandstone sample against temperature and pressure.

The behavior observed in these two figures are clear evidences of the local fluid flow mechanism.

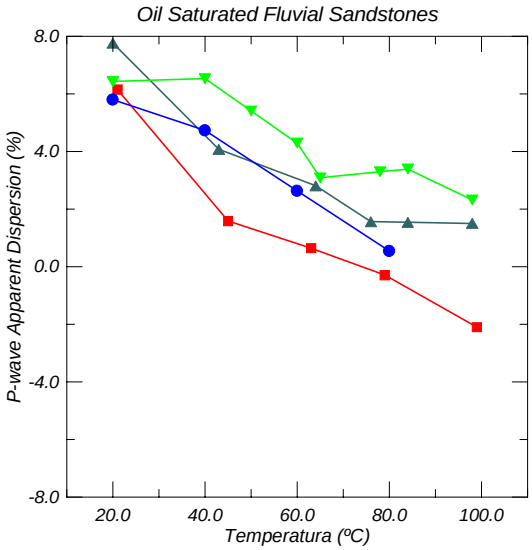


Figure 7 - Apparent and Biot dispersion versus temperature for fluvial sandstone samples.

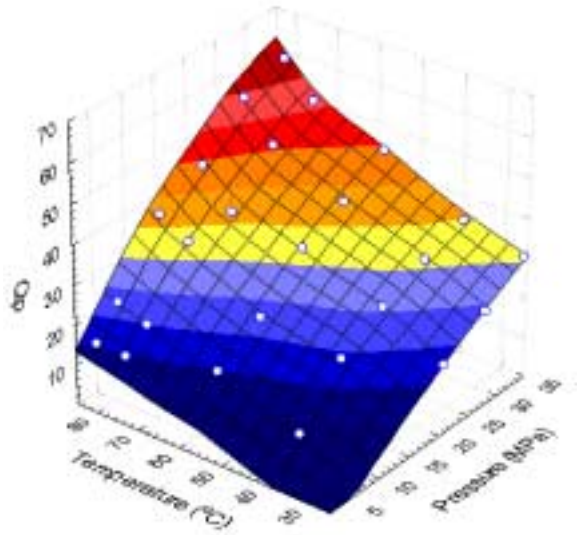

Figure 8 - Compressional wave quality factor against temperature and pressure for a turbiditic sandstone sample.

The compressional wave velocity of an oil saturated fluvial sandstone sample are plotted in figure 9 as a function of temperature, with the maximum local flow and the Biot theory predicitons. It seems that the local flow mechanism becomes less important for higher temperatures, as expected.

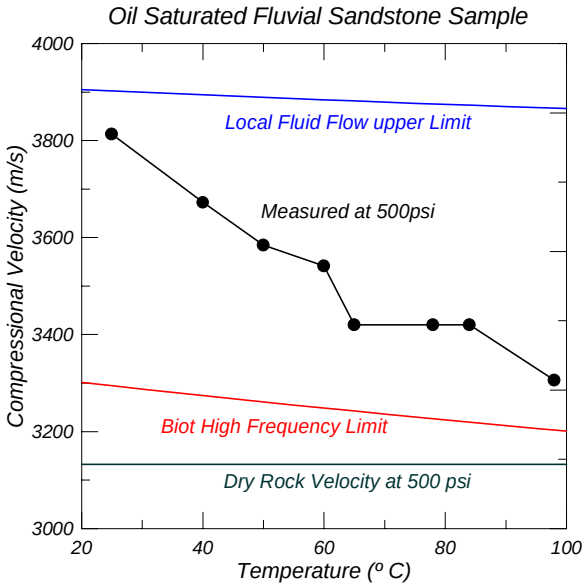


Figure 9 - Measured P-wave velocity of an oil saturated sample versus temperature.

## Conclusions

The velocities and quality factors of Brazilian sandstones and its relationships with the facies attributes were investigated. The results shows that the local fluid flow is more important than the global flow at high frequencies, specially with viscous saturating fluids, as expected. Velocities and quality factors seems to be influenced mainly by porosity, cementation and clay content. The results observed shows slightly different behavior for each data set, indicating the importance of different laboratory studies for different reservoirs.

## References

Batzle, M. L., and Wang, Z., 1992. Seismic properties of pore fluids: *Geophysics*, **57**, 1396-1408.

Biot, M. A., 1956. Theory of propagation of elastic waves in a fluid saturated porous solid, II, Higher frequency range: *J. Acoust. Soc. Am.*, **28**, 179-191.

Mavko, G. and Jizba, D., 1991. Estimating grain-scale fluid effects on velocity dispersion in rocks: *Geophysics*, **56**, 1940-1949.

Toksöz, M. N. , Johnston, D. H. and Timur, A., 1979. Attenuation of seismic waves in dry and saturated rocks: I. Laboratory measurements. *Geophysics*, **44**, 681-690.

Wang, Z. and Nur, A., 1990. Dispersion analysis of acoustic velocities in rocks. *J. Acoust. Soc. Am.*, **87**, 2384-2395.